Visual Recognition of Electrical Discharges by Video Processing

Narges Sabeti

Submitted to the
Institute of Graduate Studies and Research
in partial fulfillment of the requirements for the Degree of

Master of Science
in
Electrical and Electronic Engineering

Eastern Mediterranean University
August 2014
Gazimağusa, North Cyprus

Approval of the Institute of Graduate Studies and Research

Prof. Dr. Elvan Yılmaz
Director

I certify that this thesis satisfies the requirements as a thesis for the degree of Master of Science in Electrical and Electronic Engineering.

Assoc. Prof. Dr. Hasan Demirel
Chair, Department of
Electrical and Electronic Engineering

We certify that we have read this thesis and that in our opinion it is fully adequate in scope and quality as a thesis for the degree of Master of Science in Electrical and Electronic Engineering.

Asst. Prof. Dr. Suna Bolat
Supervisor

Examining Committee

1. Assoc. Prof. Dr. Hasan Demirel

2. Asst. Prof. Dr. Suna Bolat

3. Asst. Prof. Dr. Rasime Uyguroğlu

ABSTRACT

Electrical discharge has many fractal characteristics such as its sound and light besides from its electrical properties. In this study, partial discharge recognition is carried out by its visual light characteristics. Partial Discharge (PD) is an electrical discharge that is seen only at a part of the insulator between two conducting electrodes without completely bridging the gap. Partial discharge can occur in voids or liquid suspension in solid insulation, along the interfaces of multi-layer solid insulation systems, in gas bubbles in liquid insulation or around an electrode in a gas. Partial discharge causes deterioration and may lead to a complete breakdown of the system in time. Since partial discharge might be very destructive to power systems, it is very important to understand the mechanism of partial discharge.

In this study, a technique for visual recognition of partial discharges by video processing is introduced. Required data for the study is obtained experimentally, because PDs are highly complex and it is difficult to study analytically. A measuring system; a regular camera to capture images along with the high voltage measurement apparatus, is installed for experimental study. High AC voltage is applied to two different electrode configurations. PD is intentionally generated by using rod-plane electrode system and recorded by the camera. Acquired data is then used for recognition of PD by using video processing techniques. The correlation between visual images of PD and applied voltage during a discharge is investigated. The effect of electrode separation on PD images is also examined. Different electrode systems are designed by using two different profiles for the rod electrode. These configurations are tested and, PD images are captured by regular camera and stored

in order to carry out some analysis by video processing to get more information on PD phenomena. As a result of video processing, informative data about PDs such as propagation and light intensity of PD can be achieved.

The possibility of detection, classification, diagnostics and monitoring by video processing for PD studies is investigated in this thesis. Therefore, by understanding the discharge mechanism, identification, quantification and risk assessment of insulation defects in power system will be feasible.

Keywords: Partial discharge, corona, visual recognition, video processing.

ÖZ

Elektriksel boşalmalar elektriksel özelliklerinin yanısıra, ses ve ışık gibi pek çok ayrımsal özelliğe de sahiptir. Bu çalışmada, elektriksel boşalmanın tanınmasında görsel ışık karakteristikleri kullanılmıştır. Kısmi Boşalma (KB), iki iletken elektrot arasındaki yalıtkanın yalnızca bir bölümünde gerçekleşen, bütün açıklığı köprülemeyen, elektriksel bir boşalmadır. Kısmi boşalmalar, katı yalıtkan içindeki boşluklarda veya sıvı asıltılarda; çok katmanlı katı yalınkanlarda, yalıtkan arayüzeylerinde, sıvı yalıtkanda bulunan gaz kabarcıklarında veya gaz içinde bulunan elektrot etrafında oluşabilir. Kısmi boşalmalar sistemde bozulmaya ve zamanla delinmeye yol açabilir. Kısmi boşalmalar güç sistemleri için çok zarar verici olduğu için, kısmi boşalma mekanizmasını anlamak çok önemlidir.

Bu çalışmada kısmi boşalmaların video işleme ile görsel tanınması için bir teknik tanıtılmıştır. Gerekli veriler deneysel olarak elde edilmiştir çünkü KBlar çok karmaşıktır ve analitik olarak incelenmeleri çok zordur. Deneysel çalışmalar sırasında boşalma görüntülerini kaydetmek için sıradan bir kamera ve yüksek gerilim ölçme araçlarıkullanılmıştır. Yüksek AC gerilimler, iki farklı elektrot sistemine uygulanmıştır. KB üretmek için çubuk ve düzlem elektrotlar kullanılarak farklı elektrot düzenleri oluşturulmuş ve KB görüntüleri kamera ile kaydedilmiştir. Elde edilen veriler daha sonra KBların video işleme ile tanınması için kullanılmıştır. Görüntüler ve boşalma sırasındaki uygulanan gerilim arasındaki ilişki araştırılmıştır. Farklı elektrot düzenleri oluşturabilmek için, iki farklı çubuk elektrot biçimi tasarlanmıştır. Elektrot açıklığının KB görüntülerindeki etkisi de bu çalışmada incelenmiştir. Bu düzenlerde deneyler yapılmış ve KB görüntüleri bir kamera

yardımıyla kaydedilmiştir. KB olayları ile ilgili daha fazla bilgi sahibi olmak için video işleme tekniğiyle bazı analizler yapılmıştır. Video işleme sonucunda KB ile ilgili bilgi verici, boşalma şiddeti, ışığın yayılması ve ışık şiddeti gibi parametreler elde edilebilir.

Bu çalışmada, video işleme yöntemi ile KB varlığı belirleme, KB sınıflama, KB tanısı ve sistem izleme olasılıkları incelenmiştir. Böylece, boşalma mekanizmasının anlaşılmasıyla, güç sistemlerinde yalıtkan kusurlarının tanıması, nicelemesi ve risk değerlendirmesi gerçekleştirilebilir.

Anahtar Kelimeler: Kısmi boşalma, korona, görsel tanıma, video işleme.

ACKNOWLEDGMENT

During my studies in EMU as Master student, I had the endless support and encouragement from my supervisor Asst. Prof Dr. Suna BOLAT. She inspired me in many ways... Day and night she answered all my questions with everlasting patience. She help me through the entire process, guided me in my courses, my assistanship and my research. I had a great opportunity to start a laboratory with her which gave me great deal of experience. Not only in my academic life, but also in my personal life she has a great impact. I will never forget this excellent atmosphere she provided me with her guidance and care. I would never have been able to finish this study without her supervision. Her experience and knowledge is the base of this thesis. Thanks for everything!

Special thanks to Assoc. Prof. Dr. Hasan Demirel who was always willing to help me with his great suggestions.

Finally, I would like to thank my husband who is always there for me, my parents and my older sister for their support and encouragement.

TABLE OF CONTENTS

LIST OF TABLES

LIST OF FIGURES

LIST OF SYMBOLS

a	Electrode space
d	Distance
E	Electric field
E_c	Onset electric field
F	Total electric force
h	Height of conductor
P	Pressure
q	Source charge
Q	Test charge
r	Radius
T	Temperature
V	Voltage
V_c	Corona onset voltage
W	Weight
δ	Relative air density
ρ	Charge density
Φ	Flux of electric field

LIST OF ABBREVIATIONS

AC	Alternating Current
BD	Breakdown
DGA	Dissolved Gas Analysis
EMI	Electro Magnetic Interface
FEM	Finite Element Method
GIS	Gas Insulated Substation
HPLC	High Performance Liquid Chromatography
HV	High Voltage
HVT	High Voltage Transformer
PD	Partial Discharge
RGB	Red Green Blue
UV	Ultra Violet

Chapter 1

INTRODUCTION

1.1 Motivation and Thesis Objective

In modern world, electricity is the most significant source for many facilities. However, the quality of power from the grid should be stable to sustain those facilities, especially some factories and buildings need constant power and the cost of power outages might be catastrophic for them. In this sense, monitoring and protection of power system are extremely vital in power system development. When the high voltage technology was developed to generate and transmit the power at the beginning of the last century, partial discharges (PD) are an insidious parameter for insulation failure in high voltage (HV) equipment. These issues emphasize the importance of studying the behavior of electrical discharges within insulators.

PD is a discharge activity that does not bridge the electrodes of an insulation system under high voltage. PD normally occurs across defect sites, such as cavities, voids, joints, cracks, and delimitations. PD is initiated when the local electrical field intensity exceeds the electric strength of the dielectric involved, resulting in localized ionization and breakdown. Although PD does not cause immediate breakdown, it can affect the insulation performance in long term and might cause energy loss and gradually degrade the insulation system [1]. Also, under certain conditions, PD might lead insulation system to breakdown completely due to repetition of partial discharge [2]. Depending on the intensity, partial discharges are often accompanied by

emission of heat, very distinctive sound and light, and radio influence voltage with wide frequency range. The term of PD includes different type of discharges such as:

- Corona discharge in gases.
- Treeing channel.
- Surface discharge at interfaces.
- Internal discharge in voids or cavities within the dielectric.

As mentioned above, since PD has emission of light, feasible pattern recognition can be assessed experimentally. Visual detection of a PD and then identification, classification, possibly localization of discharges can be achieved by using image processing and video processing which allow considerable improvement in diagnostics of solid insulation systems. A lot of methods have been reported on detecting and measuring PD activity within insulation system in the past and present and a review of these methods is detailed in Chapter 2.

In this study, visual detection of PD activity has been performed with regular camera for different electrode configurations. Different electrode configurations are installed to create discharges intentionally. Under AC and DC high voltages, by changing the voltage level, the distance between camera and test object and the electrode gap, various discharge videos have been recorded and a dataset has been obtained. All videos have been processed using video processing techniques to assess PDs characteristic and classification of different discharge types. Using discharge videos or images, it is possible to identify the effects of different factors on PDs characteristics. The main objectives of this thesis are as below:

- To increase the understanding of PD phenomena.
- To identify critical parameters of PD through visual detection such as magnitude, intensity and propagation.
- To classify partial discharges.
- To compare the effect of electrode gap on visual characteristic of PDs.
- To assess the effect of distance between camera and test object on PD light.

1.2 Organization of Thesis

A brief review of the partial discharge term, how to model it and necessity of detecting PDs, is presented in Chapter 2. Also in this chapter, the effect of PD in insulating system is investigated and at the end all methods of measuring and detecting partial discharges are criticized with their advantages and disadvantages. Theoretical background is explained in Chapter 3. In Chapter 4, the structure of the video processing and the algorithm of this study are introduced. Chapter 5 consists of the computational results based on three corona light parameters by video processing and their comparison for two different electrode systems. Finally, the thesis will finish with conclusion and future study in Chapter 6.

Chapter 2

LITERATURE REVIEW

2.1 Partial Discharge

IEC standard 60270 defines partial discharge as follows: "*Partial discharge is a localized electrical discharge that only partially bridges the insulation between conductors and which may or may not occur adjacent to a conductor.*" [3]. Partial discharges are caused by the electric field intensity. When it exceeds a critical value of dielectric strength, a discharge might be observed. Partial discharges appear in very short time duration (in the range of nano second) as voltage or current impulse forms [3]. In general, partial discharge activity can be noticed in high voltage equipment such as cable, transformer, bushing, switchgear and etc.

2.1.1 PD Classification

Generally, two main groups are represented for partial discharge phenomena which are internal partial discharge and external partial discharge. Internal partial discharge occurs inside of insulation system such as cavity discharge and treeing channel. External partial discharge happens outside of equipment such as corona and surface partial discharge. Different types of PD can be seen in Fig. 2.1.

2.1.1.1 Internal Discharge

In solid or liquid insulation systems, PDs usually start within gas-filled voids due to lower dielectric constant of the void compared to surrounding dielectric in the presence of electric stress [3-4]. For better understanding of above-mentioned event, the modelling of PD is essential. A lot of research has been noticed on modelling of

partial discharge in voids within dielectric insulation system but the most famous PD model is called ‘abc’ model that introduced three capacitance models [4-8].

2.1.1.2 Treeing Channel Discharge

Electrical treeing is a continuous partial discharge that propagates through the solid insulation due to sharp edges and degenerate material. The formation of this erosion channels are similar to tree. This type of PD is very likely to destroy the insulating material [9-10].

2.1.1.3 Corona Discharge

Molecules are ionized in the air when the conductor electric filed exceeds ionization level that is called corona. Corona discharge produces sound, a distinctive smell due to ozone generation and blue-purple light. Corona can be visible at night. This phenomenon takes place where the conductor has a small curvature radius such as sharp edges corners, joints, rough conductor’s surface broken string and etc. The charge density is increased when the curvature radius is decreased, so at this area the electric field becomes considerably higher than the rest of the system therefore it can produce corona discharge [11-13]. Corona can occur in any steps of design, manufacturing, installation and maintenance of a device if there is a problem there. Corona does not attack directly to insulation system but it has indirect effect with ozone generation by corona and it can deteriorate insulating material in time which is called aging [14].

2.1.1.4 Surface Discharge

Surface discharges occur on dielectric material interface of solid insulators surface. Surface discharge can be seen on cables (mainly overhead line strings), bushing and between insulators surface such as high voltage terminals and ground. The conductive layer can be formed on insulator surface due to increasing hydrophobicity

loss in the presence of pollution under long term humidity. The rate of surface discharge can grow to generate a flashover (full line-to-ground discharge) [15].

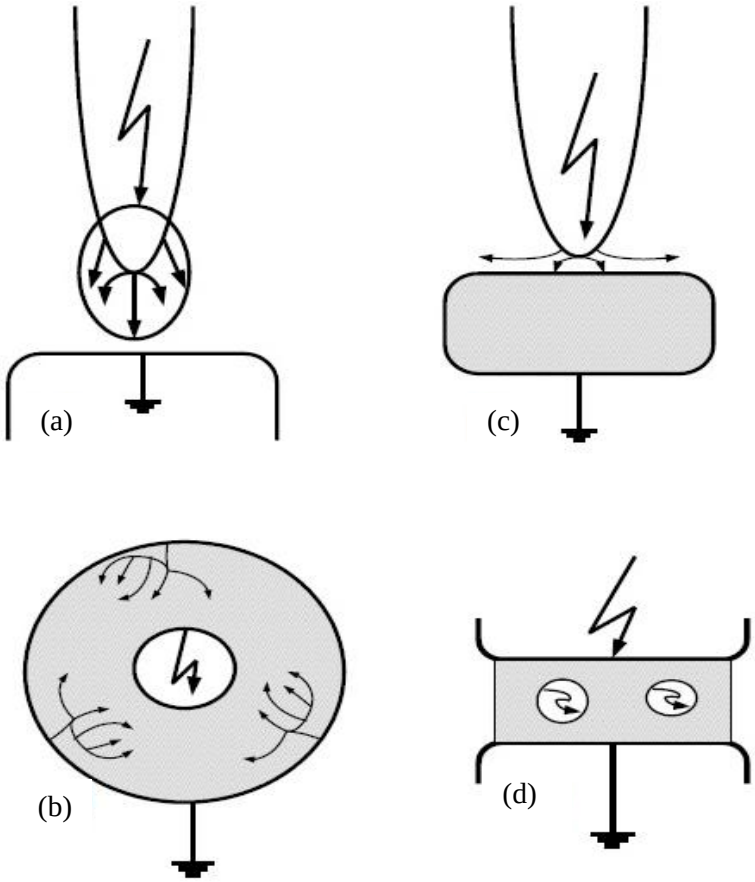

Figure 2.1. Different types of PDs: (a) Corona, (b) Treeing, (c) Surface discharge and (d) Internal discharge [16]

2.1.2 PD Effect on Insulation System and Necessity of PD Detection

Generally Partial Discharge activity generates different energy losses such as heat, light and sound depending on PD type. However, heat dissipation is the most important energy loss that causes degradation in insulation system due to chemical changes in insulation material. The effect of heat is well-known as thermal effect on insulation system so monitoring of PD phenomenon is essential time to time in manufacturing or regular check. In fact, in long operation period of HV equipment,

PD detection and measurement are always considered as critical points to secure all high voltage equipment [16].

2.2 Detection Methods of PD

Partial discharge can be detected by on electrical and non-electrical methods. The most famous PD detection methods can be divided in four groups: electrical detection method, chemical detection method, acoustic detection method, optical detection method. Depending on the characteristic of power equipment, and insulation system the method can differ.

2.2.1 Electrical Detection

The occurrence of partial discharge creates the electrical signal in type of impulse current and voltage due to short current steamer in the void within nanoseconds [17]. The pulse has some information such as its shape, its phase, location and intensity that all lead to distinguish PD and level of insulation damage. Electrical detection has two different types in order to detect signal. First method is apparent charge measurement and second one is to discover electromagnetic radiation with frequency antenna or probe [18]. This type of detection has limitation due to its tendency to noise. HV environment contains both broad band and narrow band electrical noises and however it is not easy to separate PDs from noises, this type of detection is still widely used in power plants as a popular method in online PD detection.

2.2.2 Chemical Detection

PD can create a chemical effect on insulation system due to current steamer across cavity. In fact this current can break down the material of insulator into various chemical components. Therefore PD can be detected chemically as well. Chemical detection method is very common on the oil insulated transforms. Power companies mostly use two primary chemical tests which are high performance liquid

chromatography (HPLC) and dissolved gas analysis (DGA) [19-23]. In DGA method, when PD takes place in oil-insulated device, some chemical reactions release for instance carbon oxide, methane or hydrogen. This test identifies levels of those gases in oil which are produced by the mineral oil breakdown in the transformer. Also the type of partial discharge can be distinguished with the different levels of dissolved gases but the location of PD cannot be determined [24]. HPLC method measures the byproducts of the insulation on transformer wall [20]. Chemical detection has two drawbacks, first, this method does not give any information about location of PD and its characteristic, second chemical testing cannot be done online and mostly the transformer must be taken out of operation to get oil sample which is very costly. Hence these difficulties limit the usage of this method in industry.

2.2.3 Acoustic Detection

Acoustic detection records the acoustic signals generated by the mechanical wave around corona location due to small explosion air. This method has many advantages over electrical methods due to its immunity to electromagnetic interference (EMI) [24] Acoustic emission method heavily depends on the background noise; on the other hand, signals do not have enough intensity to identify. Therefore, to detect corona and its differences one should use a sensor that can detect small changes in signal amplitude. Moreover, it is not very effective to determine the exact location of corona in non-homogenous environment [16]. Acoustic detection is generally used in high voltage transformers and gas insulated substations (GIS).

2.2.4 Optical Detection

Optical detection as it name suggest depends on the light of the discharge. When discharge occurs, during ionization, discharge light is dissipated. Corona activities

emit radiation in visible, ultraviolet and infrared optical signals. Therefore one may use different types of cameras to detect different optical signals. The light emission is dependent on some parameters such as insulating material, temperature, humidity and pressure. The detection of UV light during daylight is possible due to solar-blind UV range [25] but visible light of corona is detectable more effectively during night because of its blue-purple color. Visible light can be captured by regular camera which is much more economical than UV cameras and infrared cameras and it is possible to use video processing for online detection. According to all above-mentioned reasons visual detection can be considered as the most effective method in online detection of corona discharges.

The visual detection results are reliable and have some information about location and intensity of corona light and propagation of the discharge. Magnitude of corona however cannot be measured by optical methods. Since the apparent charge or current measurements are not possible, visual detection cannot be used for insulator maintenance or replacement decisions [26]. However, in a controlled environment with necessary measurements, the correlation between discharge magnitude and visible light of corona can be determined and visible light characteristics can then be used as a diagnostic tool.

The visual detection results are reliable and have some information about location, intensity of corona light and propagation of the discharge but still there are no information on the magnitude of corona discharge. It is difficult to make decision on insulator maintenance or replacement by visual detection since the magnitude of the discharge is not available [26]. However, in a controlled environment with necessary measurements, the correlation between discharge magnitude and visible light of

corona can be determined and visible light characteristics can then be used as a diagnostic tool.

This study proposes a method using video processing to perform corona detection and identification. In this study, a regular camera is used to capture the visual light of corona. The identification has been carried out in the manner of visible light characteristics such as propagation, intensity and area growth of light. Using blue-purple color of the discharge, the discharge zone is defined and characteristic parameters are determined. The effect of applied voltage, electrode gap and electrode type is investigated in this study. It has been noted that, there is a considerable change in corona light under different conditions.

Chapter 3

THEORETICAL BACKGROUND

3.1 Electric Field & Gauss' law

To calculate the force exerted by some electric charges, q1, q2, q3 ... as the source charges on the test charge Q, the principle of superposition can be applied. The total force exerted is equal to the vector sum of all forces exerted by q1, q2, and q3 on Q. The force exerted by a charged particle on another charged particle depends on their separation distance, velocities and accelerations [27].

The electric field at a particular point is a vector whose magnitude is proportional to the total force acting on a test charge located at that point, and its direction is equal to the direction of the force acting on a positive test charge. The electric field $\vec{E}$, generated by a collection of source charges, is defined as:

$$\vec{\mathrm{E}} = \vec{\mathrm{F}}/_{Q} \tag{3.1}$$

where F is the total electric force exerted by the source charges on the test charge Q. The total force exerted by the source charges on the test charge is equal to:

$$\begin{aligned} \vec{\mathrm{F}} = \overrightarrow{F_1} + \overrightarrow{F_2} + \overrightarrow{F_3} + \cdots &= \frac{1}{4\pi\varepsilon_0}\left(\frac{q_1 Q}{r^2{}_1} + \frac{q_2 Q}{r^2{}_2} + \frac{q_3 Q}{r^2{}_3} + \cdots\right) \\ &= \frac{Q}{4\pi\varepsilon_0}\sum_{i=1}^{n}\frac{q_i}{r^2{}_i}\hat{r}_i \end{aligned} \tag{3.2}$$

Therefore electric field with respect to the source charges is equal to:

$$\vec{\mathrm{E}} = {}^{\vec{\mathrm{F}}}/_{Q} = \frac{1}{4\pi\varepsilon_0}\sum_{i=1}^{n}\frac{q_i}{{r^2}_i}\hat{r}_i \qquad \textbf{(3.3)}$$

The electric field can be graphically represented using field lines. The direction of the field lines indicates the direction in which a positive test charge moves when placed in this field. The density of field lines per unit area is proportional to the strength of the electric field. The flux of electric field lines through any surface is proportional to the number of field lines passing through that surface. The electric flux through any surface that encloses the charge q is equal q/ε_0. Using the principle of superposition for more than one point charge, flux of electric field is given as:

$$\emptyset_E = \oint_{surface}\vec{\mathrm{E}}\,.\,\mathrm{d}\overrightarrow{a} = \sum_i \oint_{surface}\vec{E}_i.\,\mathrm{d}\overrightarrow{a} = \frac{1}{\varepsilon_0}\sum q_i \qquad \textbf{(3.4)}$$

Hence, for an arbitrary surface and arbitrary charge distribution:

$$\oint_{surface}\vec{\mathrm{E}}\,.\,\mathrm{d}\overrightarrow{a} = \frac{Q_{enclosed}}{\varepsilon_0} \qquad \textbf{(3.5)}$$

where $Q_{enclosed}$ is the total charge enclosed by the surface which is called **Gauss' law.** Using the divergence theorem the electric flux $\emptyset_E$ can be rewritten as:

$$\oint_{surface}\vec{\mathrm{E}}\,.\,\mathrm{d}\overrightarrow{a} = \oint_{volume}\left(\vec{\nabla}\,.\,\vec{\mathrm{E}}\right).\,\mathrm{d}\tau \qquad \textbf{(3.6)}$$

The enclosed charge $Q_{enclosed}$ can be written in terms of the charge density ρ:

$$Q_{enclosed} = \oint_{volume}\rho.\,\mathrm{d}\tau \qquad \textbf{(3.7)}$$

Then Gauss' law can change as:

$$\oint_{volume}\left(\vec{\nabla}\,.\,\vec{\mathrm{E}}\right).\,\mathrm{d}\tau = \frac{1}{\varepsilon_0}\oint_{volume}\rho.\,\mathrm{d}\tau \qquad \textbf{(3.8)}$$

Since there is not any assumption about the integration volume, integrands are equal:

$$\vec{\nabla} \cdot \vec{E} = \frac{\rho}{\varepsilon_0} \tag{3.9}$$

This equation is called Gauss's law in differential form [27].

The scalar function whose gradient is the electric field is called the electric potential V and it is defined as:

$$\vec{E} = -\nabla \vec{V} \tag{3.10}$$

This equation can be written as:

$$\overrightarrow{\nabla^2} \vec{V} = -\frac{\rho}{\varepsilon_0} \tag{3.11}$$

That is known as Poisson's equation. The electric potential generated by a discrete charge distribution can be obtained using the principle of superposition:

$$V_{total} = \sum_{i=1}^{n} V_i \tag{3.12}$$

where V_i is the electric potential generated by the point charge q_i:

$$V_i = -\frac{1}{4\pi\varepsilon_0} \int_{\infty}^{r} \frac{q_i}{r^2} \mathrm{d}r = -\frac{1}{4\pi\varepsilon_0} \frac{q_i}{r} \tag{3.13}$$

The total electric potential generated by the whole set of point charges is equal to [27]:

$$V_{total} = -\frac{1}{4\pi\varepsilon_0} \sum_{i=1}^{n} \frac{q_i}{r} \tag{3.14}$$

3.2 Electric Field and Geometric Shape

Electric field between two conductors changes depending on the geometric shape of the conductor. Electric field lines and equipotential lines are always perpendicular, i.e. there is always 90° between them. Electrode surface is also an equipotential line, therefore electric field lines heavily depend on the geometry of the electrode. If the conductor has a homogenous surface, the field distribution is uniform e.g if it is

spherical; the electric field vectors should cross the center of the sphere since they are perpendicular to the spherical surface. If the conductor has non-homogenous geometry, the electric field vector at any point is perpendicular to the tangent line at that point. As a result, the electric field has the strongest intensity at points along the surface where the object has the smallest curvature radius. Sharp points, corners, edges create strong electric fields [28] because of their small curvature radius compared to the rest of the electrode. The differences in the field intensity for sharp tip and round tip electrodes can be seen in the Fig 3.1.

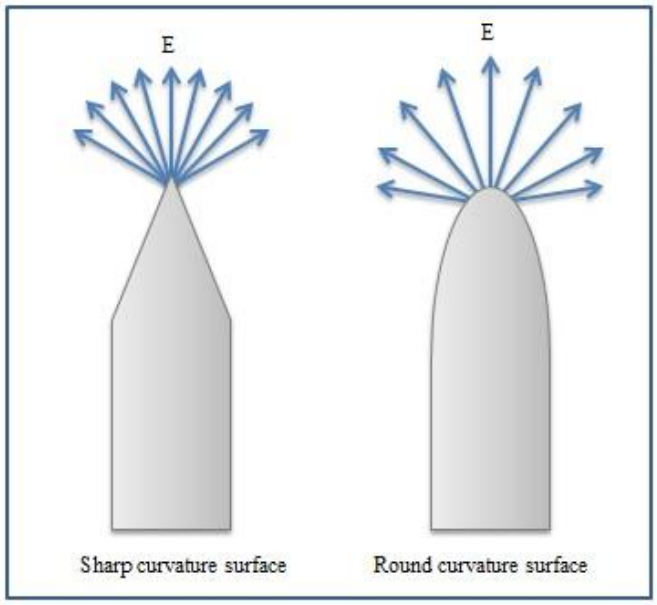

Figure 3.1. Electric field upon the surface

3.3 Non-uniform Field for Gas

Generally, a discharge initiates when the electrical stress exceeds certain level called breakdown strength. Any kind of gas can withstand stress up to a critical value. Since, for uniform field gap the stress is the same everywhere, discharge is expected to occur in a form of complete breakdown. However, in non-uniform field gaps, the discharge takes place only in the areas where the stress is higher than the rest of the

insulation which is called partial discharge. Corona is a partial discharge that occurs in air or other gases [29].

3.3.1 Corona Types

- Positive corona: The discharge is formed on the positively charged conductor (e.g., during the positive half-wave voltage). It is generally found in areas with sharp edges, corners. The visual appearance of this corona type is small region of a glow around a certain location. This is a relatively weak source of corona discharge, and it creates a slight sound [29].
- Negative corona: This type of corona occurs on the negatively charged, conductor for example, during the negative half-wave voltage. It looks like a flame with constantly changing shape, direction and size. This corona is very sensitive to changes in the environmental parameters. Its appearance gives rise to an acoustic tone around the double-frequency (e.g. 100 Hz) of the electric field [29].

3.3.2 Corona Onset Voltage & Field

Corona onset field is the critical stress value at the conductor surface when the corona is initiated and corona onset voltage is the minimum discharge voltage corresponding to the corona inception. Onset electric field E_c and the corona onset voltage V_c are calculated for different configuration [29].

3.3.2.1 Single Conductor above Ground (wire-plane)

The critical field E_c which causes stable corona on the conductor is given as:

$$\mathrm{E_c} = 30\mathrm{m_s}\delta + \left(1 + \frac{0.301}{\sqrt{\delta.\,\mathrm{r}}}\right)\ \mathrm{kV_{peak}/cm} \qquad \textbf{(3.15)}$$

where r is a radius of the conductor δ is a relative air density and m_s is a surface irregularity factor ($m_s = 1$ for smooth conductor and $m_s < 1$ for rough conductor). The corona onset voltage for this case is calculated as:

$$V_c = E_c . r . \ln\left(\frac{2H}{r}\right) \quad kV \tag{3.16}$$

where, H is the height of the conductor above ground [29].

3.3.2.2 Coaxial Cylinder

The critical field E_c for coaxial cylinder is given as:

$$E_c = 31 m_s \delta + \left(1 + \frac{0.308}{\sqrt{\delta . r_1}}\right) \quad kV_{peak}/cm \tag{3.17}$$

where r_1 is the inner radius. The corona onset voltage for this case is calculated as:

$$V_c = E_c . r_1 . \ln\left(\frac{r_2}{r_1}\right) \quad kV \tag{3.18}$$

where r_2 is the outer radius. In both cases δ is relative air density is given as:

$$\delta = \left(\frac{P}{P_0}\right)\left(\frac{T_0}{T}\right) \tag{3.19}$$

where $T_0$is the absolute room temperature and $P_0$is the normal atmospheric pressure, T is the actual temperature and P is the pressure of the air [29].

3.3.2.3 Rod-Plane Electrode System

Utilization factor, η of an electrode arrangement having non-uniform field is given as:

$$\eta = {E_{mean}}/{E_{max}} \tag{3.20}$$

where E_{mean}, is the average field strength of the arrangement over the electrode gap and $E_{max}$is the highest field strength occurring in the field region. Utilization factor changes $1 \geq \eta > 0$. At uniform field, η is equal to 1, at non-uniform field is smaller than 1 [30].

Using utilization factor η of electrode configuration, corona onset voltage, V_c or corona onset field strength E_c can be calculated. For example, corona onset voltage in a SF6 insulated system in a non-uniform field can be expressed as below [30]:

$$V_c = 0.8775\ \eta.S.C.P.a \quad kV \tag{3.21}$$

where η is an utilization factor; S is the electrode surface roughness factor (s < 1), C is the curvature factor (depends upon the shape and size of electrodes), P is gas pressure in kPa and a electrode spacing in cm.

The corona onset field strength can be calculated from experimental V_c values by [30]:

$$E_c = {}^{V_c}/_{\eta.a} \tag{3.22}$$

where a the electrode spacing and η is the utilization factor.

3.3.2.4 Numerical Solution of Rod-Plane Electrode System

The Finite Element Method (FEM) is a powerful numerical method for solving physical problems. In the finite element method, the model is divided into separate finite elements, connected to each other in nodes. The connected finite elements create a mesh of the studied model. The problem then can be solved for one element at a time. After that, solution is recombined to have a complete solution. In the corona discharge problem, a fine mesh is used close to the emitting electrode, because a large gradient of the electric field is required [31].

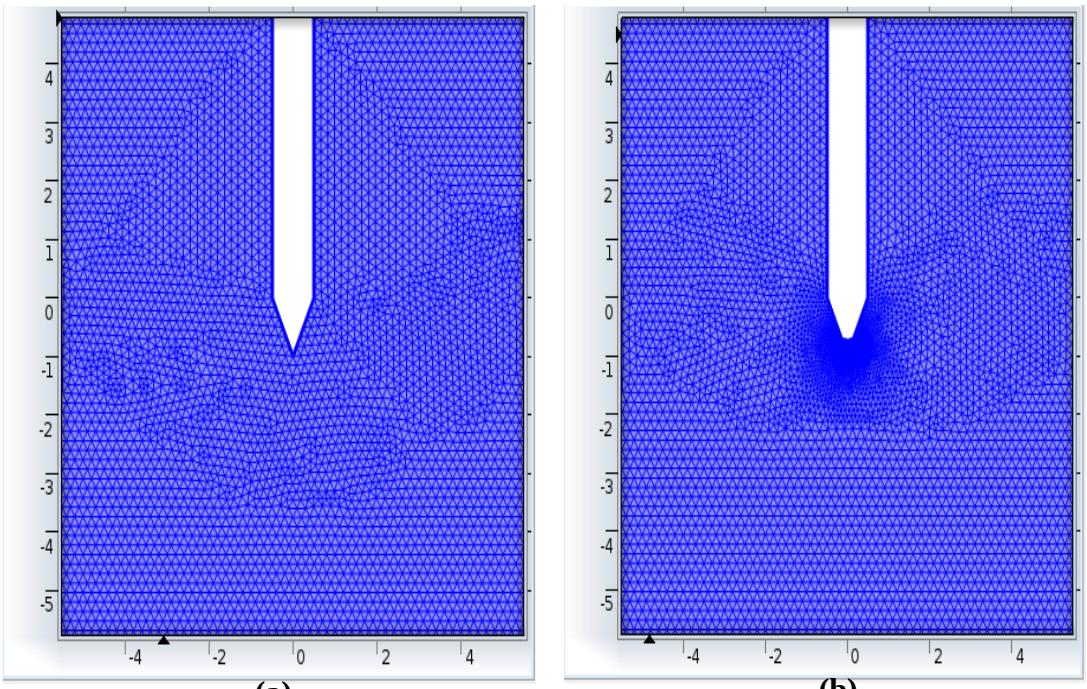

Figure 3.2. The electrode systems with their meshes (a): Sharp tip electrode (b): Round tip electrode.

The rod-plane electrodes used in the experiments are analyzed numerically by Finite Element Method. Two electrodes, with the same length of 5 cm and 1 cm thickness, having a different curvature radius at the tip are shown in the Fig. 3.2 with their meshes.

For simulation, the mesh is chosen to be extremely fine. The equations are based on Gauss' law and Poisson's equations. Electric field intensity and energy density are observed at specific point on the top of two curvature tip models to study the effect of sharpness on corona phenomenon. The electric field distribution and energy density distribution for two electrode configurations are shown in Figs 3.3 to 3.6 respectively.

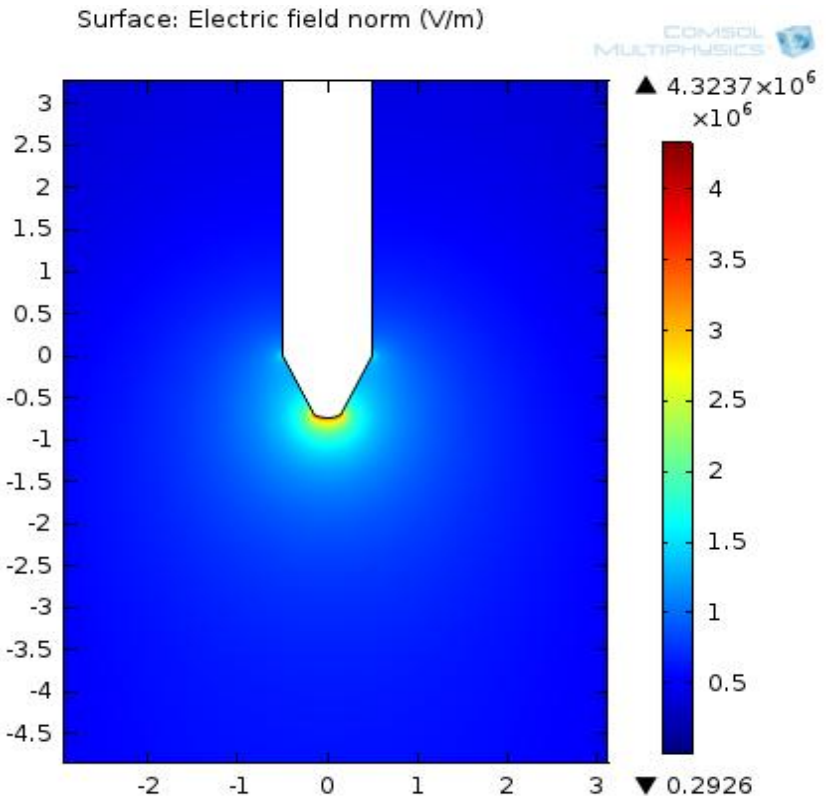

Figure 3.3. Electric field distribution for round-tip electrode

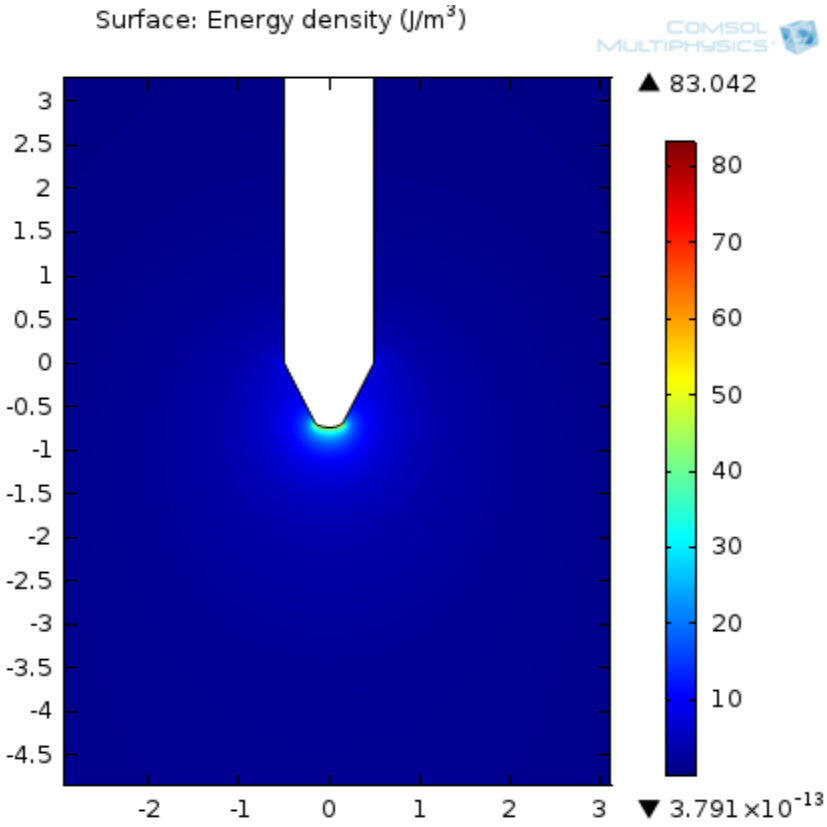

Figure 3.4. Energy density distribution for round-tip electrode

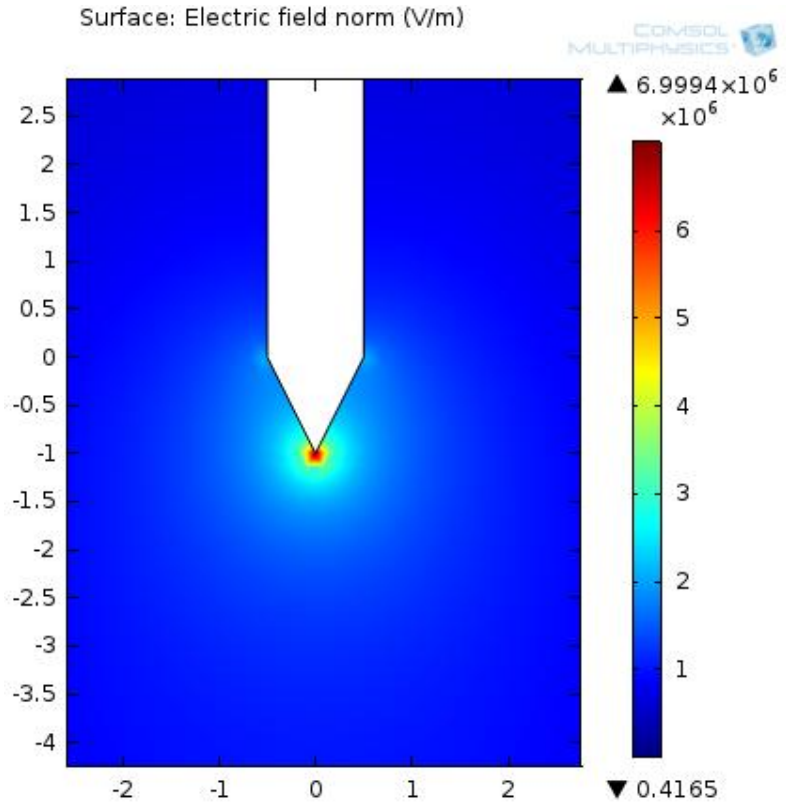

Figure 3.5. Electric field distribution for sharp-tip electrode

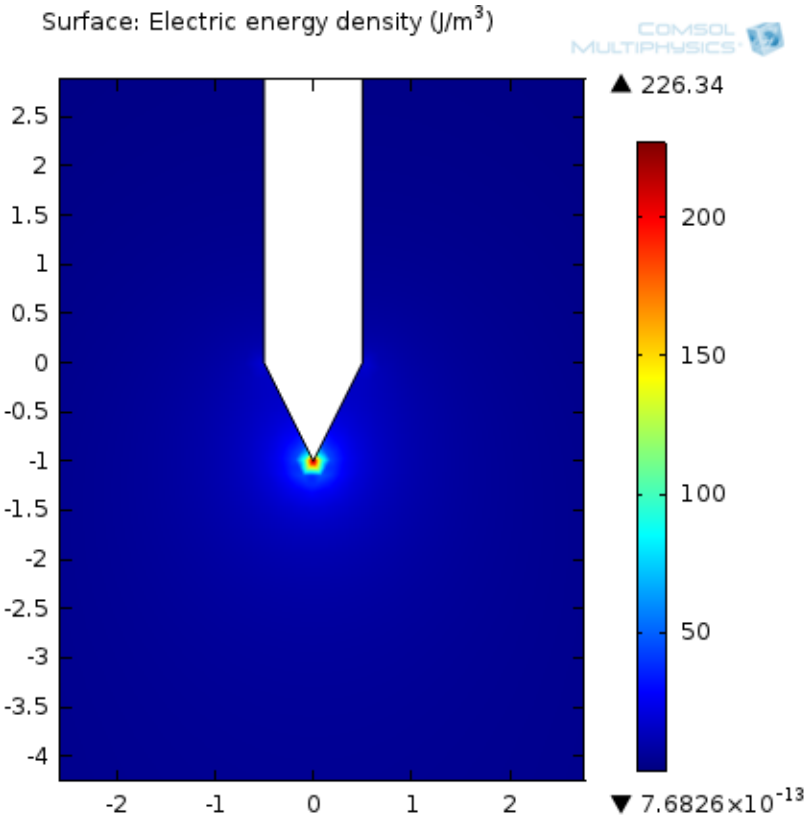

Figure 3.6. Energy density distribution for sharp-tip electrode

Table 3.1. Electric field norm **(V/m)** with respect to applied voltage for round -tip electrode and Sharp-tip electrode of **5cm** electrode gap

	Electrode curvature	
Applied voltage (kV)	**Round-tip electrode** (V/m)	**Sharp-tip electrode** (V/m)
45	2.90750 e^6	3.40706 e^6
50	3.58558 e^6	3.78562 e^6
55	3.94413 e^6	4.16418 e^6
60	4.30269 e^6	4.54274 e^6
65	4.66125 e^6	4.92130 e^6
70	5.01981 e^6	5.29986 e^6
75	5.37836 e^6	5.67843 e^6
80	5.73692 e^6	6.05699 e^6
85	6.09548 e^6	6.43555 e^6
90	6.45404 e^6	6.81411 e^6

Table 3.2. Electric energy density ($\mathbf{J/m^3}$) with respect to applied voltage for round -tip electrode and Sharp-tip electrode of **5cm** electrode gap

	Electrode curvature	
Applied voltage (kV)	**Round-tip electrode (J/m^3)**	**Sharp-tip electrode (J/m^3)**
45	37.42625	51.39166
50	56.91630	63.44650
55	68.86873	76.77026
60	81.95948	91.36295
65	96.18855	107.22458
70	111.55596	124.35513
75	128.06168	142.75462
80	145.70574	162.42303
85	164.48812	183.36037
90	184.40883	205.56665

The result of the simulation is geometry-sensitive: the calculated electric field intensity and electric energy density values are bigger for sharp-tip electrode under same level of voltage. Moreover both parameters increase with increasing the applied voltage.

Chapter 4

VIDEO PROCESSING AND METHODOLOGY

4.1 Video Processing

The videos of electrical discharges are recorded by camera and then converted into frames using a built-in MATLAB function in this study. For cost-effective results, 1920×1080 resolution is used. Image matrix contains enough information and matrix dimension is small enough to avoid big computational time with this resolution.

A video is a sequence of images called frames in which each frame is a monochrome or full-color image. An image can be defined depending on resolution. Every single element in an image is called pixel. Pixels are arranged in rows and columns. Therefore, the total number of pixels in the image presents a matrix, letting an image to be represented by a two-dimensional matrix (M×N) [32]. The horizontal rows of pixels are called lines and the vertical columns are called samples. The color image of corona is recorded for 20 seconds for different voltage levels. At first corona light should be identified then some characteristics of corona light can extracted from the videos in order to have some information on different discharges such as area growth, light propagation and light intensity of discharges.

4.1.1 Color Codes

Each pixel contains some information about the discharge such as color code, light emission and location of that pixel. To identify corona light, first of all color image processing should be applied. Color is a crucial parameter of an image and there are lots of color models, that the followings are used in this study:

- **RGB color model**: In color image processing, images can be represented by additive color model, which is called RGB (Red-Green-Blue) color model. In RGB color model, a broad array of colors can be reproduced adding red, green and blue colors in various ways. In this way, each pixel can be defined as red, green and blue components of an RGB image. Those red, blue and green components are also called as channel [32].
- **YCbCr color model**: Another color model that is experimented in this study is YCbCr model which Y represents the luminance or brightness information of light and color information is stored as two color difference components, Cb and Cr. Cb denotes the difference between blue color and a reference; Cr denotes the difference between red color and a reference [32]. For light intensity studies, YCbCr model is applied.

4.1.2 Preprocessing Data

The video recordings contain unnecessary images which are not related to corona. Therefore, before characterizing the discharge, location of the discharge is defined. First background of the test area is cleaned from the entire image and then pixels which do not belong to the discharge are dismissed from the matrix. This way, the accuracy of the identification process becomes more accurate.

4.1.2.1 Background Subtraction

Identifying moving objects from a video sequence is a fundamental and critical task in many computer-vision applications. A common approach is to perform background subtraction, which identifies moving objects from the portion of a video frame that differs significantly from a background model. In this study, the background of test area is recorded separately and one frame of background is subtracted from the entire image frame by frame. In this way, images contain corona

light and background noise but not the background itself. The procedure of background subtraction can be seen in Fig. 4.1 as below:

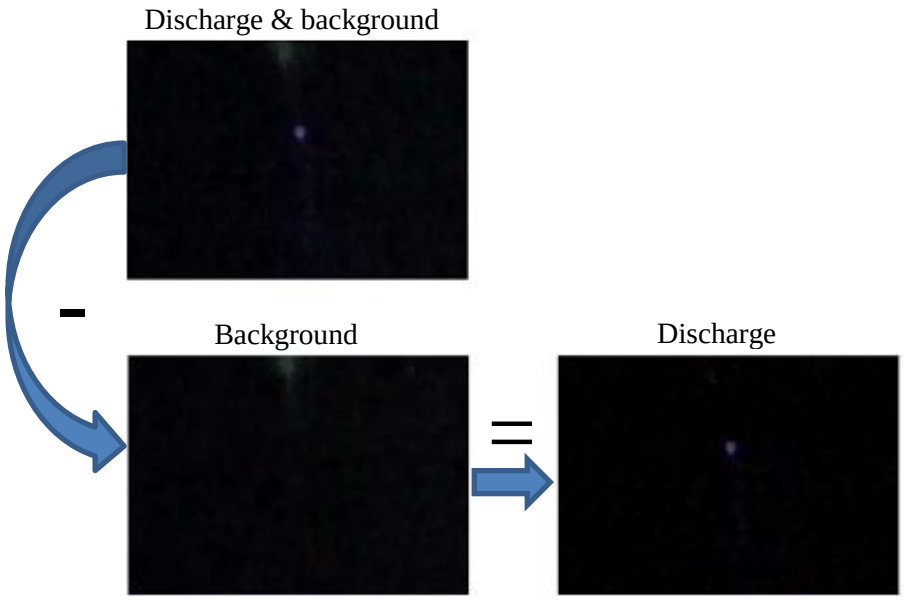

Figure 4.1. Background subtraction

All frames are cropped at the location of interest, which is close to region of discharge. After clearing the background, to identify visible corona discharge and remove background light, a threshold is applied.

4.1.2.2 Single Thresholding

In the original image, a gray level T is chosen. Then the grayscale image is converted to a binary image. After that, every pixel is turned either black or white by comparing its value to T.

A pixel becomes white if its gray level is > T

A pixel becomes black if its gray level is <= T

Global thresholding is determined by choosing threshold T that separates object from background. With global thresholding, all pixels of three colors which belong to discharge area can be detected. Blue channel, red channel and green channel of the

images have been investigated. It has been noted that, red and blue color are dominant in a corona discharge. As it is mentioned before, corona discharge has a blue-purple color. Therefore, green color is neglected during thresholding because the effect of green color in a corona discharge is small. The main purpose here is to capture all visible pixels that belong to the discharge area. If the weight of summation red and blue colors in a pixel is greater than a critical value, it is noted that this pixel belongs to corona discharge. By trial-error, histogram and CDF graphs of red and blue channel, the optimum threshold level for corona is determined to be 30 as seen in the Figs. 4.2-5. Histogram graph acts as a graphical representation of the tonal distribution. In fact it shows the number of pixels belong to each tonal value which are variable from 0 to 255. The cumulative distribution function (cdf) for the quantity gives the probability of having a critical value [32]. The x axis in empirical CDF graph shows the tonal of pixel from 0 to 255 and F(x) axis shows the probability of pixels. The histogram graph and empirical CDF graph are determined for each color channel to decide about optimum threshold level.

$$T_{corona} \rightarrow W_{red} + W_{blue} > 30 \qquad \textbf{(4.1)}$$

Where $T_{corona}$is the threshold for corona discharge, W_{red} is the weight of red is color and W_{blue} is the weight of blue color. If the summation of weight of red and blue colors in a pixel is smaller than 30, that pixel is removed from the image. All steps of thresholding can be seen in Figs. 4.2-7 including the effects of red and blue colors in a corona discharge.

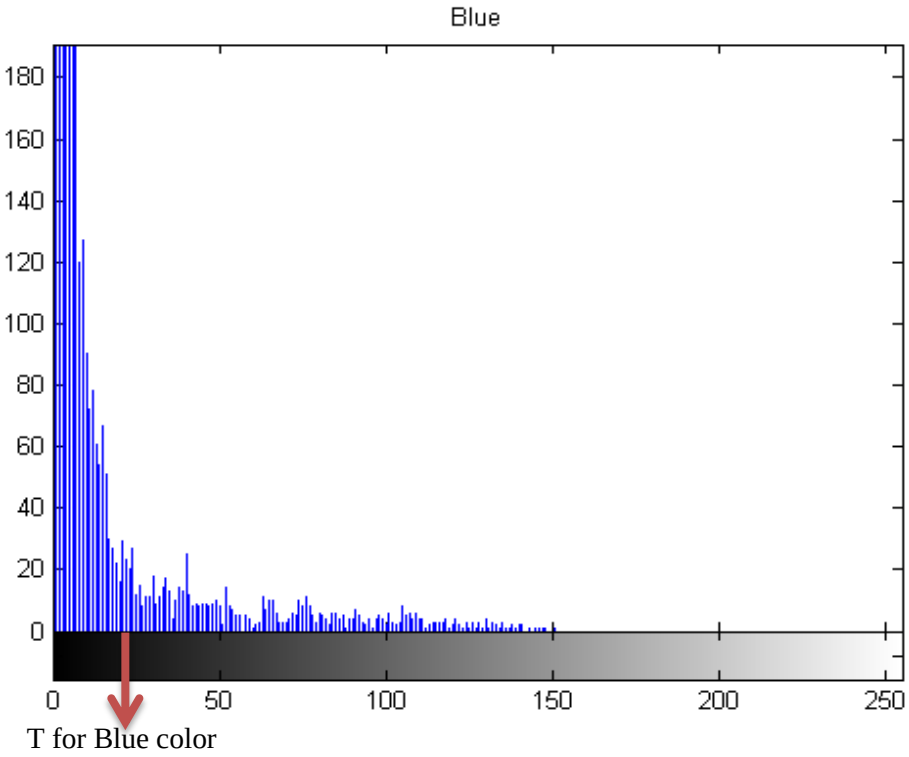

Figure 4.2. Histogram diagram of blue channel

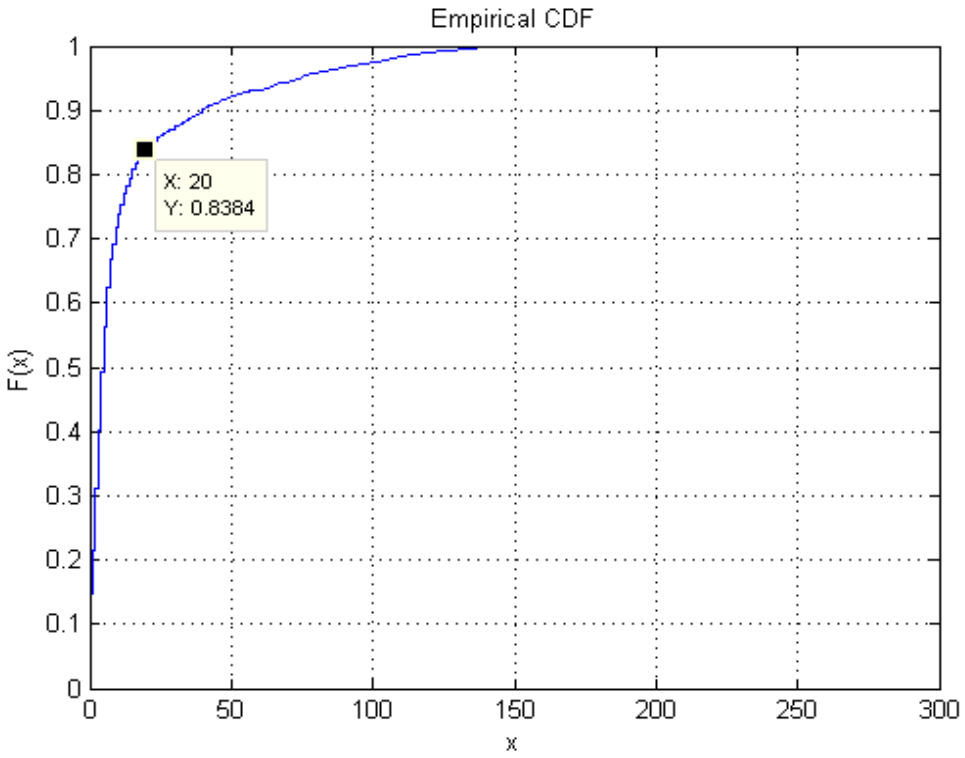

Figure 4.3. Empirical CDF diagram of blue channel

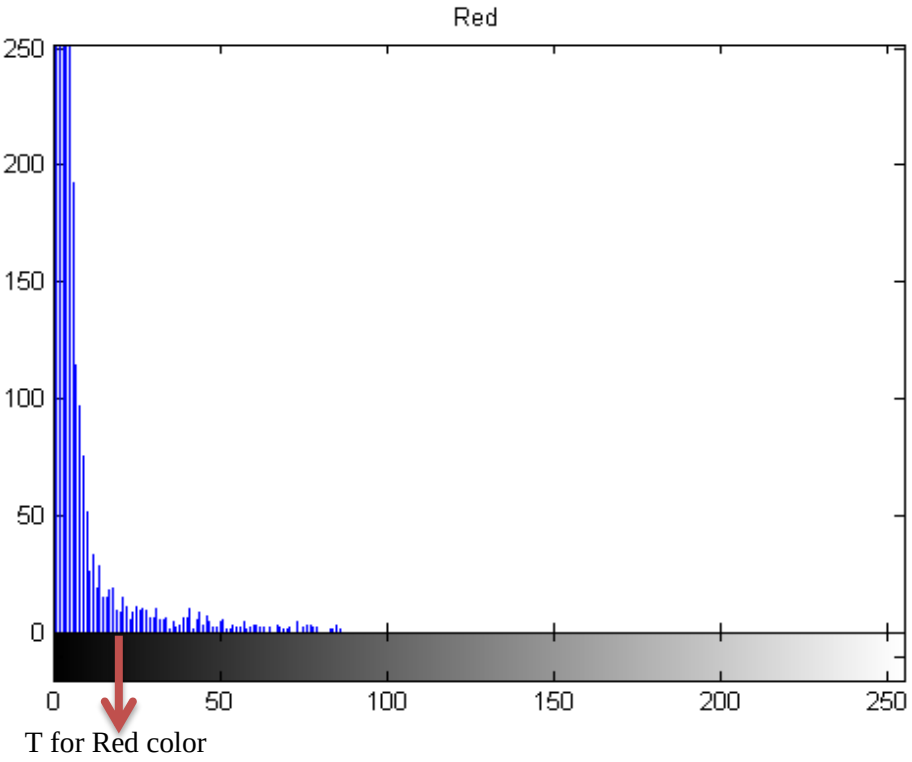

Figure 4.4. Histogram diagram of red channel

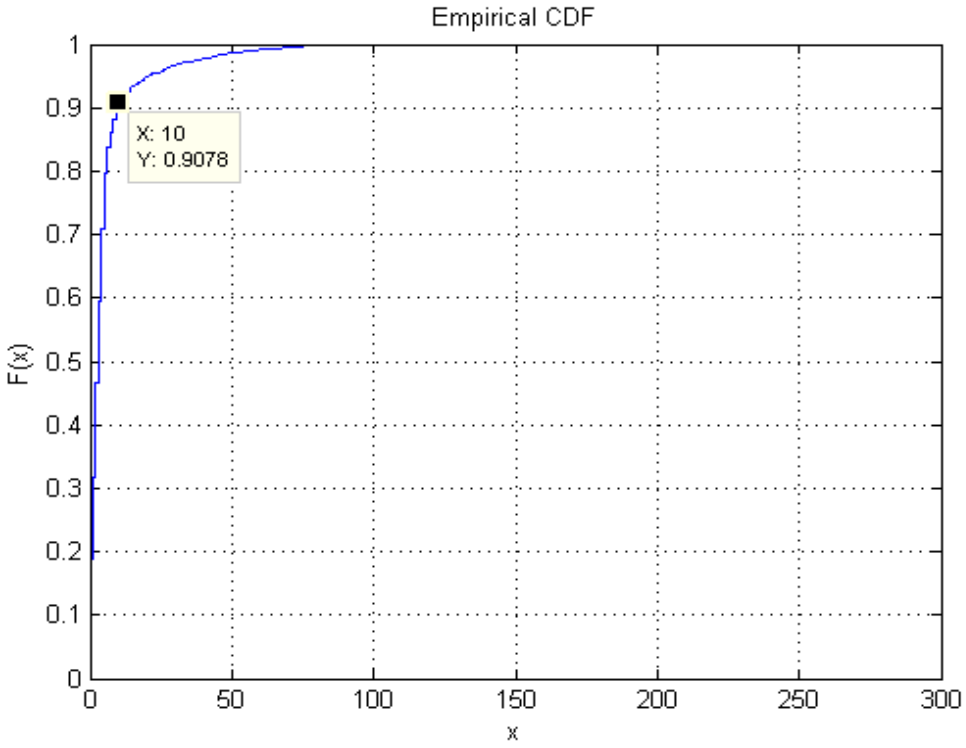

Figure 4.5. Empirical CDF diagram of red channel

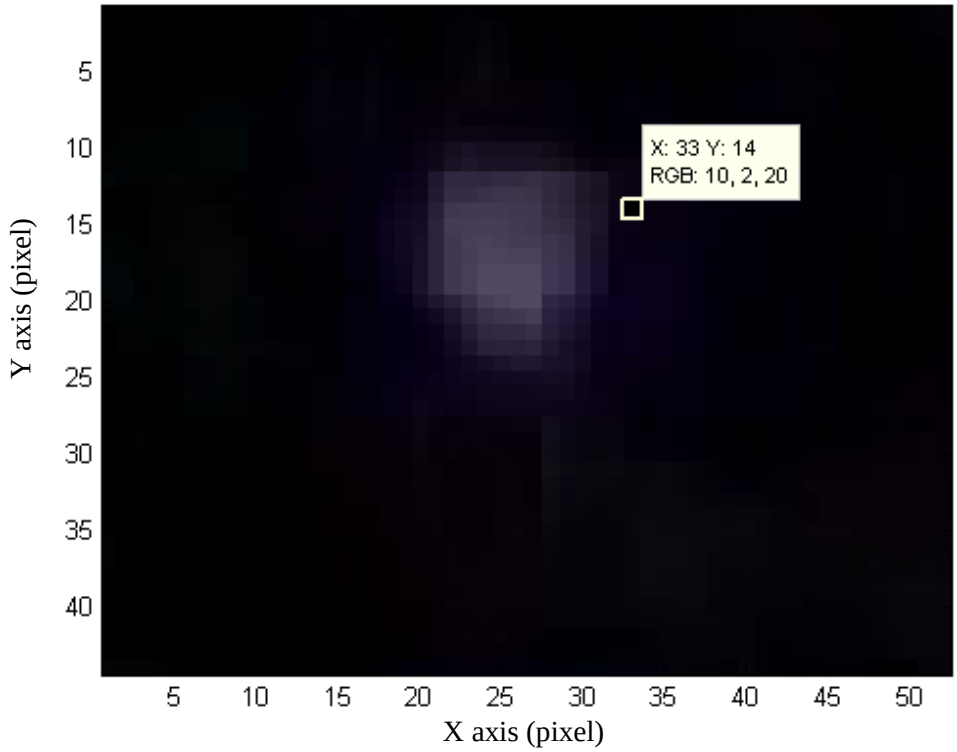

Figure 4.6. Discharge light with respect to three channels of red, green and blue colors

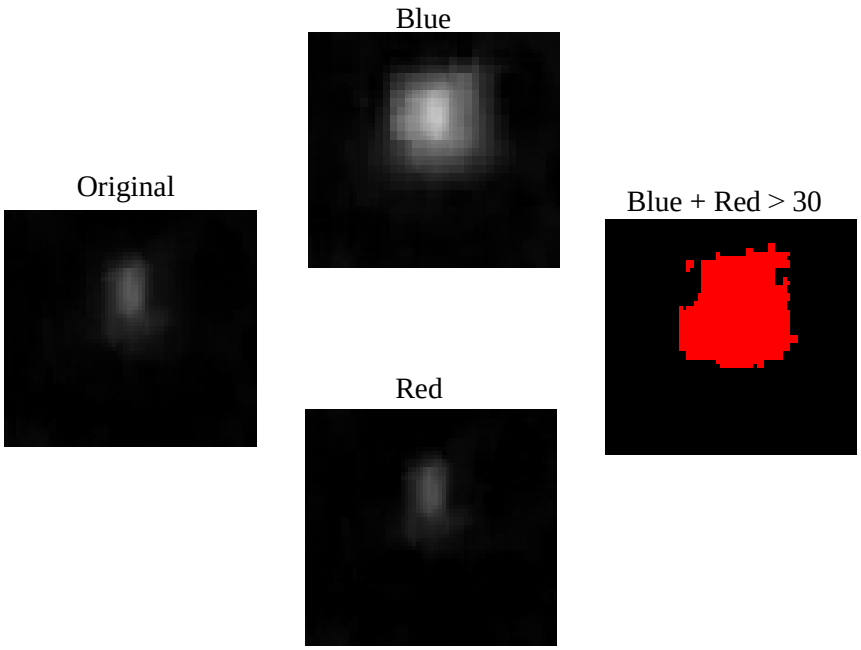

Figure 4.7. Processed discharge images

It should be mentioned that the critical value of threshold method tried for all videos that are captured in different condition due to trial-error and mentioned figures are examples to show the procedure.

4.1.3 Corona Light Characteristics

After identifying corona light, three parameters, area growth, light propagation and light intensity, are extracted from the videos in order to have some information on different discharges. Those parameters are used as an indicator to characterize a discharge.

4.1.3.1 Area Growth

Area growth represents the number of all pixels that belongs to the discharge zone [26]. First the discharge zone is defined and all the pixels belong to discharge zone is calculated to determine area growth.

4.1.3.2 Propagation

Propagation of corona light is the furthest pixel (x_i, y_i) in discharge zone to discharge center (x_c, y_c) [26]. In fact discharge center is defined as the center of discharge zone. The distance between the furthest pixel and the center is calculated by Euclidean norm:

$$\mathrm{d} = \sqrt{(\mathrm{x_i} - \mathrm{x_c})^2 + (\mathrm{y_i} - \mathrm{y_c})^2} \qquad \textbf{(4.2)}$$

To find the furthest pixel, the distance between all pixels belong to discharge zone are calculated with respect to the center then the maximum value is taken into account. Moreover, the pixel is shown with red color in discharge images to double check the furthest pixel with respect to center. Fig.4.8. shows one sample frame of furthest pixel from center of discharge.

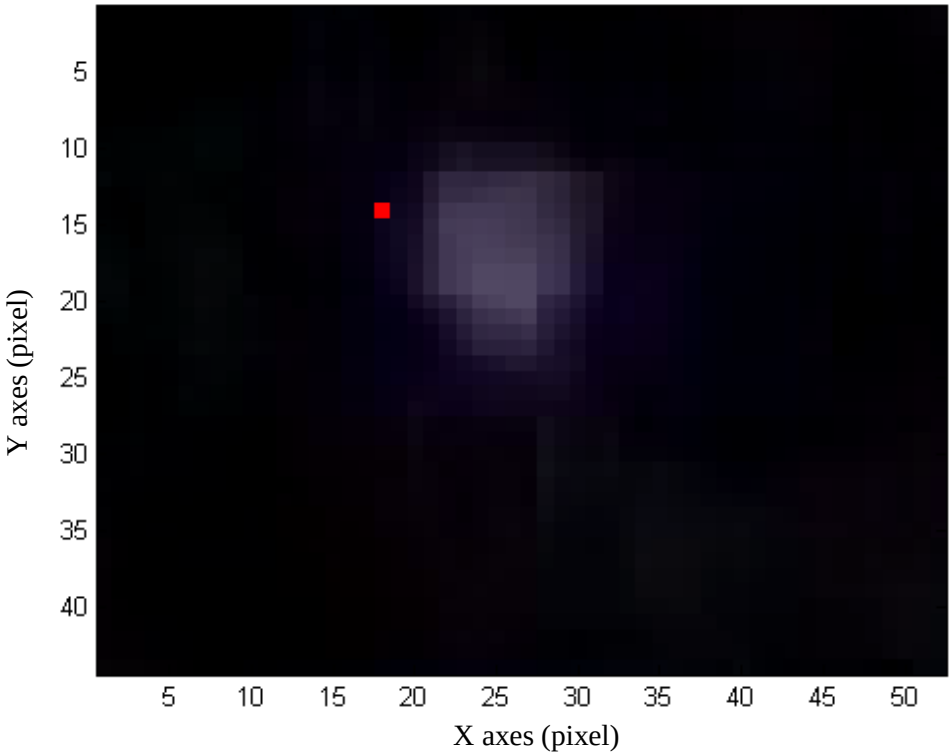

Figure 4.8. Furthest pixel from center of discharge

4.1.3.3 Intensity

Intensity of corona light is determined by the maximum luminance value of the pixel that belongs to the defined discharge zone [25]. Representing luminance of light is easier in YCbCr color space. RGB space is transformed into YCbCr color space by built-in MATLAB function. As it is mentioned before, Y represents luminance information of each pixel. Therefore, by single component of Y [32], corona intensity can be defined. The value of luminance belongs to visible discharge area is calculated as the maximum value of each frame then the average values of all frames are taken into account. Fig. 4.9 shows some samples of maximum luminance value for random frames under different levels of voltage. The index values in white boxes show luminance intensity of that pixel in each figure due to Y channel of YCbCr color

space. As it can be seen the maximum value of luminance always takes place in the center of discharge.

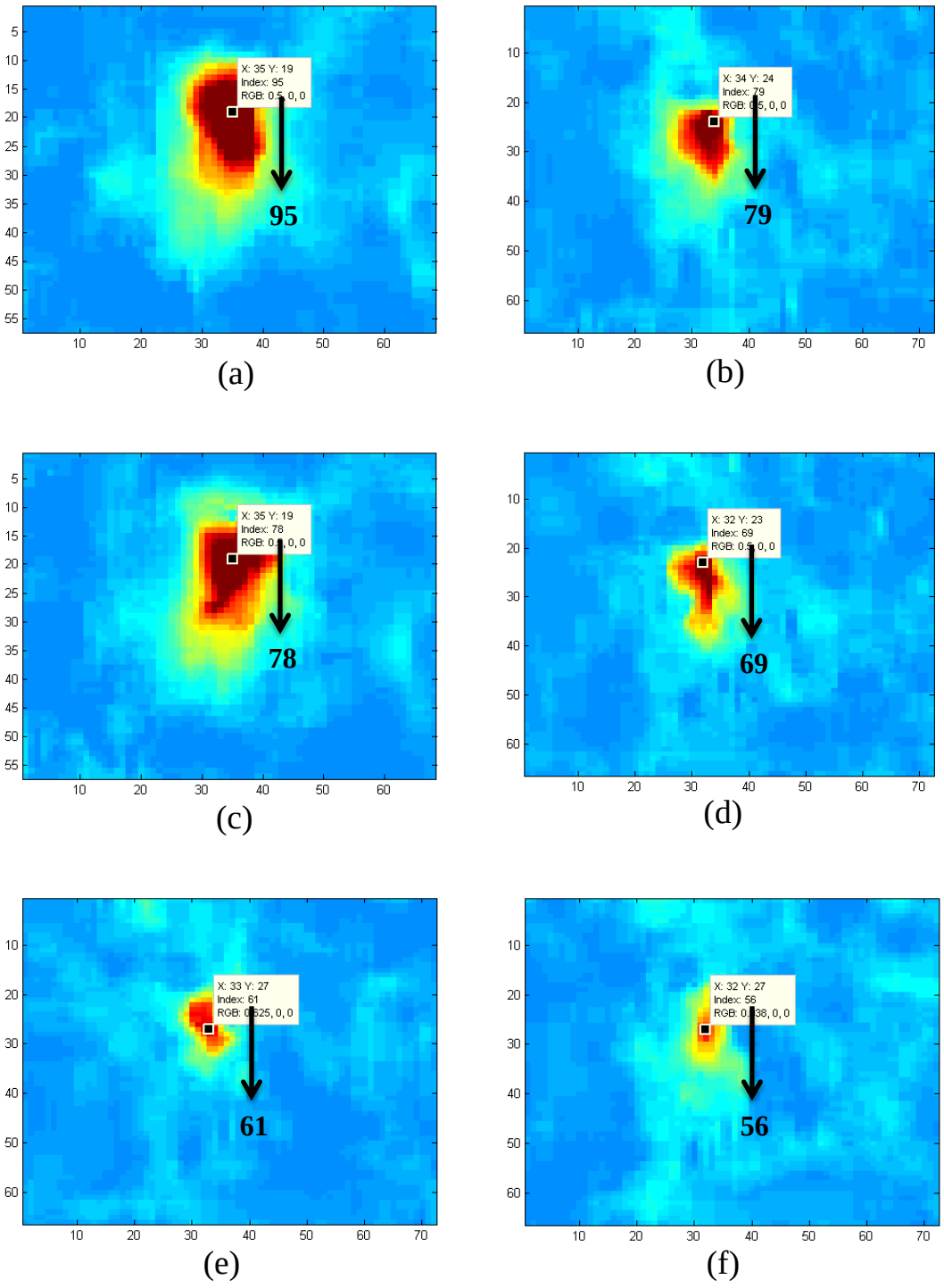

Figure 4.9. Some samples of maximum luminance value

The flowchart for video processing of corona discharge is shown in Fig. 4.10 All those steps have been carried out using MATLAB.

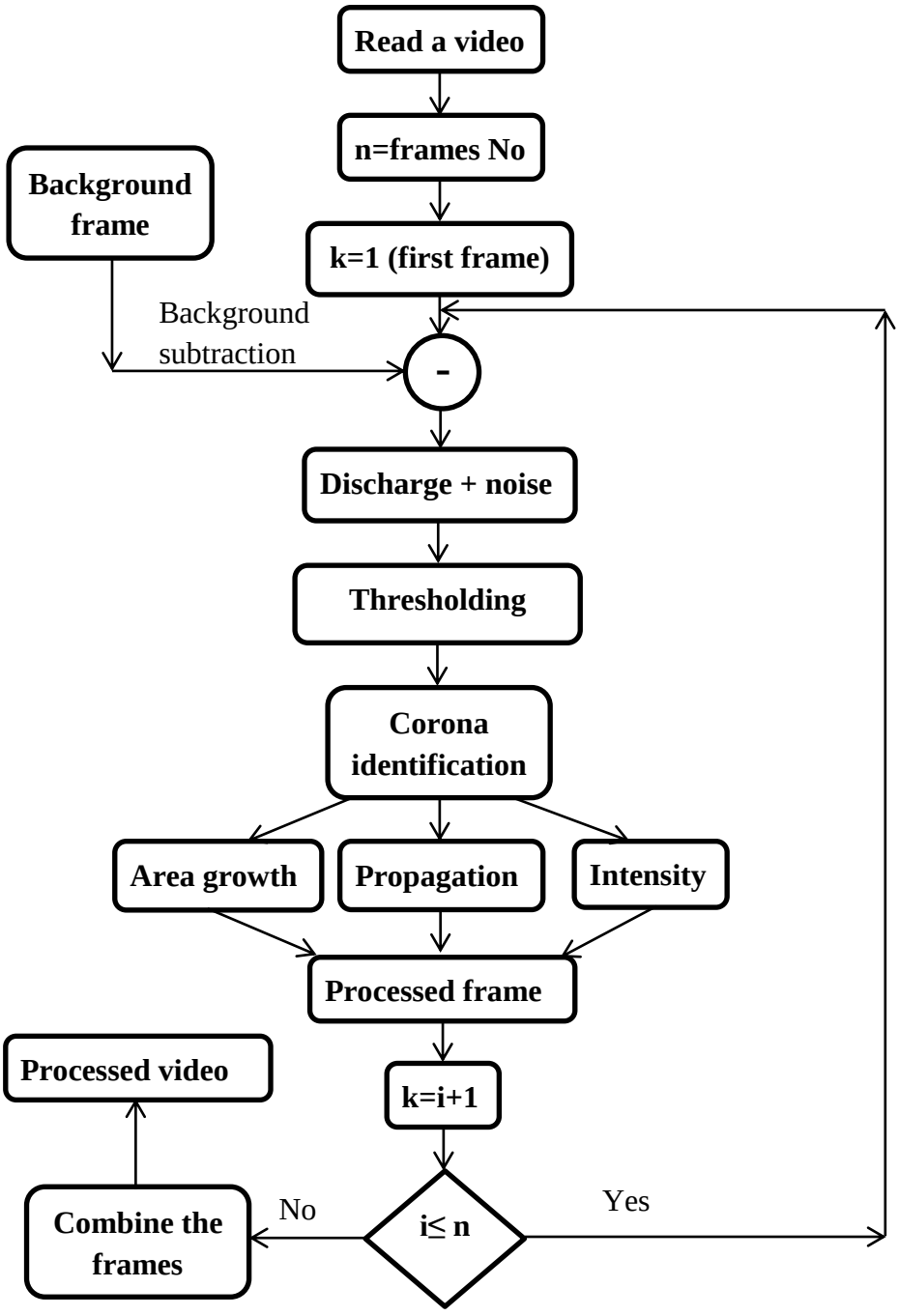

Figure 4.10. Algorithm of the methodology

Chapter 5

RESULTS AND DISCUSSION

5.1 Experimental Set up

Experiments have been carried out at High Voltage Laboratory of EMU Department of Electrical and Electronics Engineering. An electrode system is configured using a rod and a plane electrode. AC voltage is applied on the electrode system by using 5 kVA, 100 kV high voltage test transformer. The schematic diagram of experimental setup is shown in Fig. 5.1. C_1 and C_2; form a voltage divider, C_1 (100 pF) is high voltage capacitor and C_2 (0.1 μF) is low voltage capacitor, to measure the alternating voltage as seen in Fig. 5.1. The camera is installed 1 meter distant from electrode system.

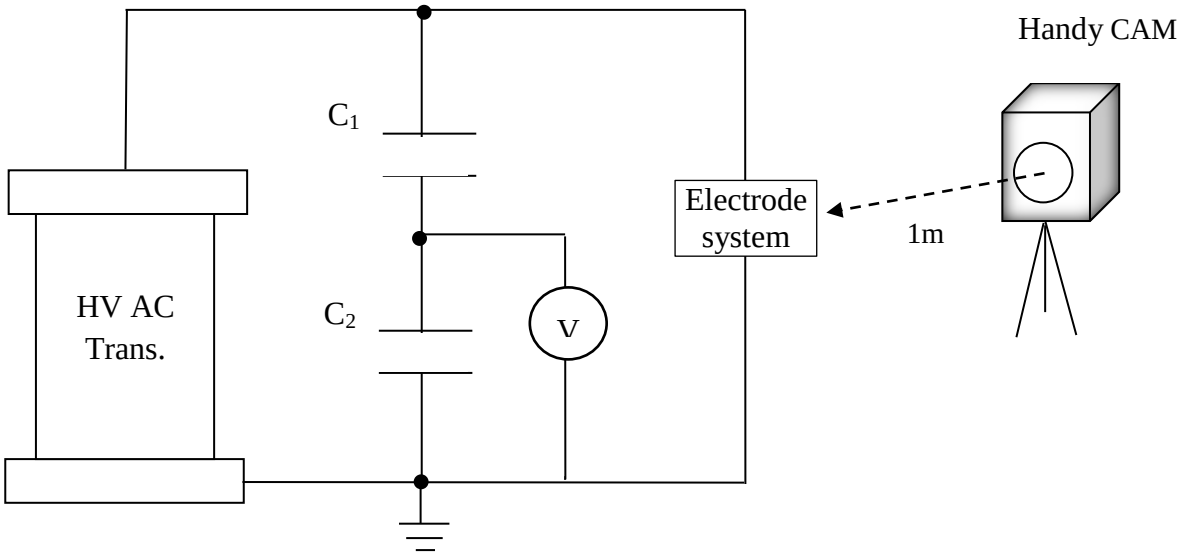

Figure 5.1. Schematic diagram of experimental setup

Figure 5.2. Experimental setup in HV laboratory

Two rod-type electrodes with the same length of 5 cm, having a different curvature radius at the tip are used in the electrode arrangement to analyze the effect of sharpness of the electrode and its influence in the corona light. Electrode system and two different electrodes used in this study are shown in Figs.5.3 and 5.4 respectively.


Figure 5.3. Electrode system

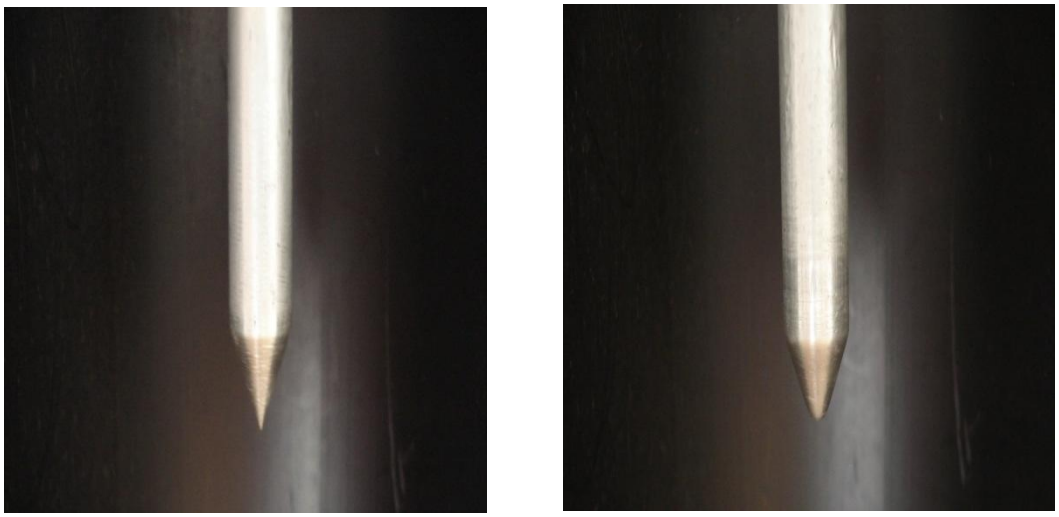

a. Electrode with a sharp tip b. Electrode with a round tip

Figure 5.4. Different rod-type electrodes used in this study

The electrode gap is adjustable. In this study, electrode gaps of 5 cm, 6 cm, 7 cm and 8 cm are tested. The applied voltage is increased in steps of 5 kV during the procedure. The light emission videos are recorded using a common camera, SONY (HDR-CX190) with 1920×1080 resolution. The camera is located at one meter distant from the electrode arrangement. The tests are performed at average air pressure of p=768 mmHg, average temperature of t = 25˚C, and average relative humidity of 40%.

5.2 Results

The experiments have been carried out in dark environment since videos are recorded by a regular camera it is not possible to capture good images in light. The characteristic parameters; area growth, propagation and light intensity of discharge are calculated for different electrodes with various separations under different voltage levels. All three parameters are calculated for each frame then the average values of them are taken into account

5.2.1 Area Growth

Area growth for sharp tip electrode is shown in the Table 5.1. This table shows that the discharge initiates sooner for smaller electrode gap as expected. In smaller electrode gaps, it is not possible to acquire many partial discharge recordings because of complete breakdown.

Table 5.1. Area growth (in pixels) of discharge zone with respect to applied voltage for different electrode gaps of sharp-tip electrode

	Applied voltage [kV]						
Electrode Gap [cm]	**40**	**45**	**50**	**55**	**60**	**65**	**70**
5	54	105	BD	BD	BD	BD	BD
6	-	64	116	125	BD	BD	BD
7	-	34	70	142	857	BD	BD
8	-	-	-	90	112	165	238

As seen in the Table 5.1, at lower voltages; the visible discharge does not start even though the discharge is audible; therefore it is not possible to record videos. At higher voltages; complete breakdown has been observed, bridging the entire electrode gap; therefore there is not any partial discharge measurements.

The average area growth increases gradually when the applied voltage is increased. In Table 5.1, it is observed that value of area growth is bigger than expected at 60 kV for 7 cm electrode gap. The reason for this anomaly is the occurrence of breakdown in the gap during experiment. Similar study has been carried out for round tip electrode. Table 5.2 shows that discharge starts at higher voltage levels and time lag for breakdown is higher compared to sharp tip electrode. From Table 5.1 and Table 5.2, it is observed that more recordings are available for round tip electrode compared to the

sharp tip electrode. Because for sharp tip electrode has stronger electric field intensity that causes sooner occurrence of complete breakdown for higher level of voltage. On the other hand, area growth of the discharge is mostly bigger for round tip electrode under same voltage. Moreover it is obvious that the area growth is bigger for smaller electrode gap under same voltage level.

Table 5.2. Area growth (in pixels) of discharge zone with respect to applied voltage for different electrode gaps of round-tip electrode

	Applied voltage [kV]									
Electrode Gap [cm]	**45**	**50**	**55**	**60**	**65**	**70**	**75**	**80**	**85**	**90**
5	140	355	634	734	BD	BD	BD	BD	BD	BD
6	-	-	169	474	655	BD	BD	BD	BD	BD
7	-	99	186	381	521	627	696	890	846	937
8	-	-	-	81	148	305	390	547	639	828

Figs. 5.5 and 5.6 show the trend of area growth for 8 cm electrode separation with both round and sharp tip rod electrodes respectively as below. It can be seen that the discharge zone gets bigger when the voltage level is increased. Figs. 5.7 and 5.8 show the same trend for 7 cm gap but the visible discharge is started at lower level of voltage in both sharp and round tip electrodes due to smaller electrode gap. Moreover at same level of voltage it is obvious that the area growth is bigger for 7 cm in both sharp and round tip electrodes. Also as it is mentioned before, there is an irregularity can be seen at 60 kV for sharp tip electrode due to complete discharge.

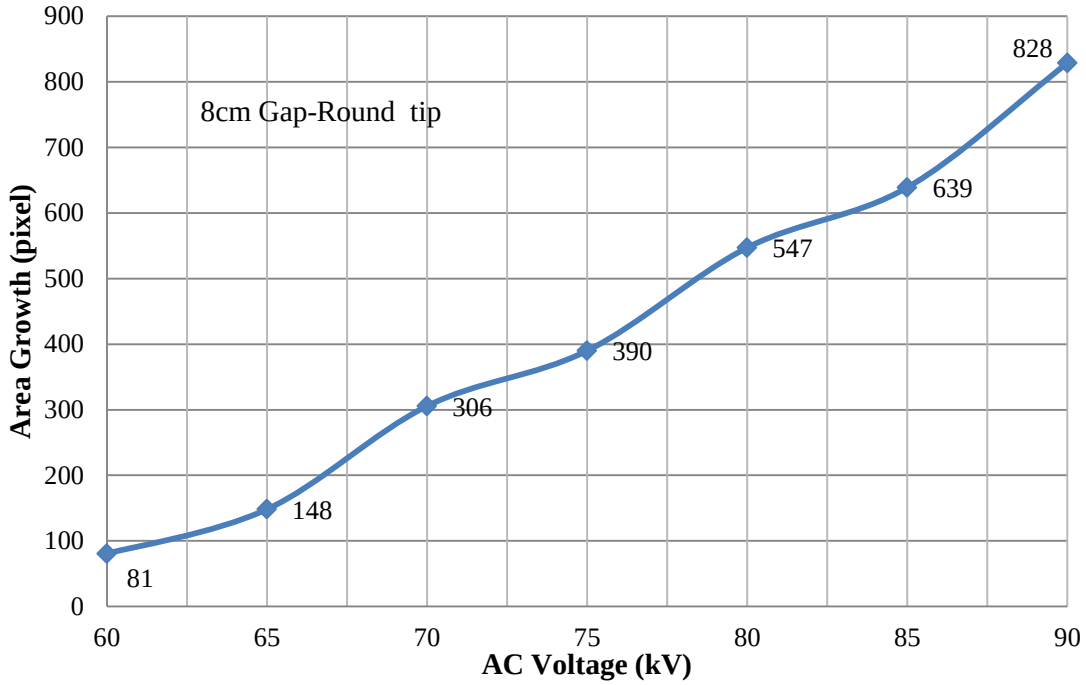

Figure 5.5. Area Growth trend with respect to applied voltage for 8 cm electrode gap with round-tip electrode

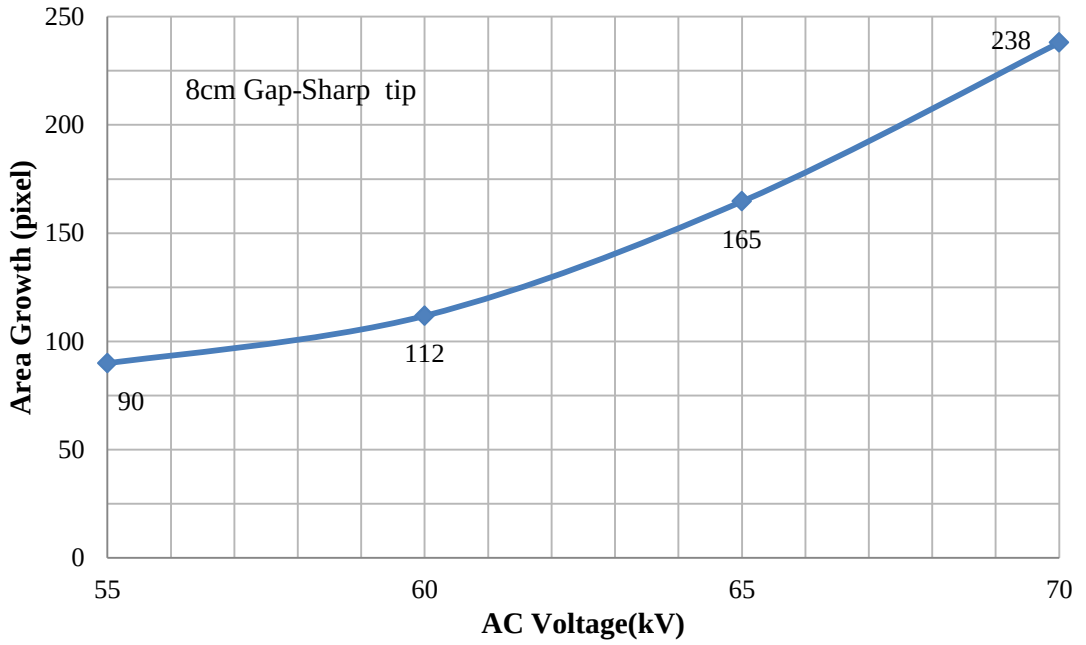

Figure 5.6. Area Growth trend with respect to applied voltage for 8 cm electrode gap with sharp-tip electrode

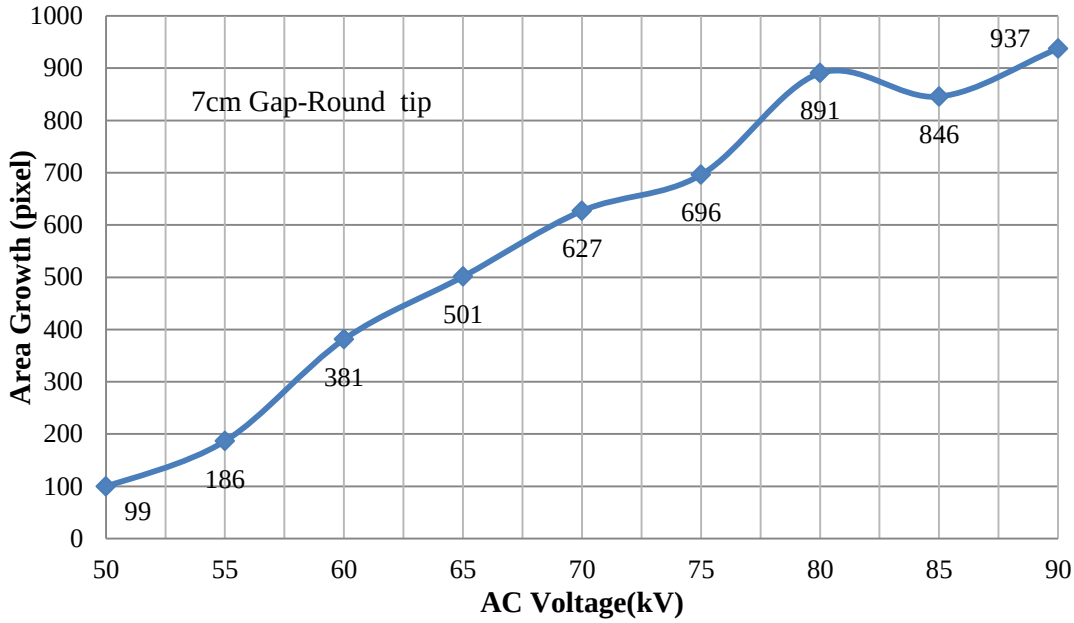

Figure 5.7. Area Growth trend with respect to applied voltage for 7 cm electrode gap with round-tip electrode

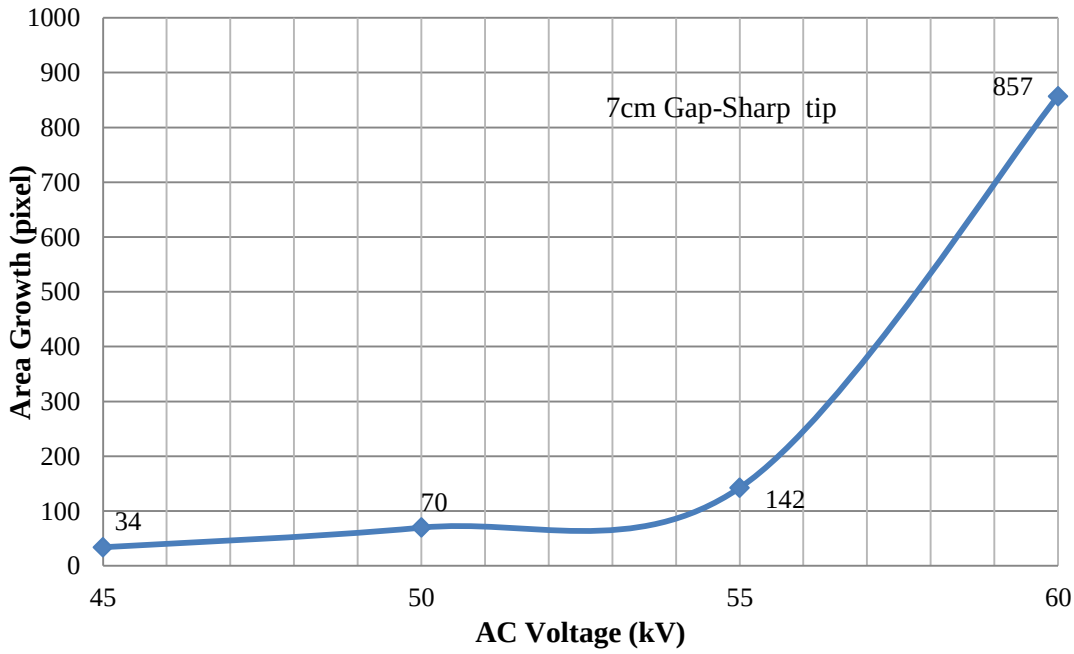

Figure 5.8. Area Growth trend with respect to applied voltage for 7 cm electrode gap with sharp-tip electrode

5.2.2 Propagation

Propagation of the discharge is represented by the distance. The average of the distance of farthest pixel belongs to discharge zone to the center for both sharp tip and round tip are shown in the tables 5.3 and 5.4.

Table 5.3. Propagation of discharge zone with respect to applied voltage for different electrode gaps of sharp-tip electrode

	Applied voltage [kV]						
Electrode Gap [cm]	**40**	**45**	**50**	**55**	**60**	**65**	**70**
5	7	9	BD	BD	BD	BD	BD
6	-	5	15	12	BD	BD	BD
7	-	5	8	12	28	BD	BD
8	-	-	-	8	9	11	18

Table 5.3 represents distance of furthest pixel to center is increased when the voltage increased. There is one abnormal value at 60 kV of 7 cm due to flashovers during experiment. On the other hand, propagation is calculated as an average value of all frames belong to each voltage level so it is expected to have some irregularities such as 55 kV of 6 cm. Same trend is observed for round tip electrode as Table 5.4.

Table 5.4. Propagation of discharge zone with respect to applied voltage for different electrode gaps of round-tip electrode

	Applied voltage [kV]									
Electrode Gap [cm]	**45**	**50**	**55**	**60**	**65**	**70**	**75**	**80**	**85**	**90**
5	13	18	24	27	BD	BD	BD	BD	BD	BD
6	-	-	16	27	23	BD	BD	BD	BD	BD
7	-	-	14	16	19	21	25	28	24	27
8	-	-	-	13	16	20	21	21	22	27

The distance of furthest pixel belongs to discharge zone to the center for both round-tip and sharp-tip electrodes at 8 cm electrode gap are shown in Figs 5.9 and 5.10. It can be seen that distance of the furthest pixel to the discharge center increases when the applied voltage increases. Figs 5.11 and 5.12 show same trend for 7cm gap. As it can be seen in the tables and figures, the number of recordings is decreased at smaller electrode gap. It is obvious that discharge starts sooner and ends sooner for 5 cm and 6 cm electrode gaps due to complete breakdown. Unfortunately there is not enough data to discuss for these observations.

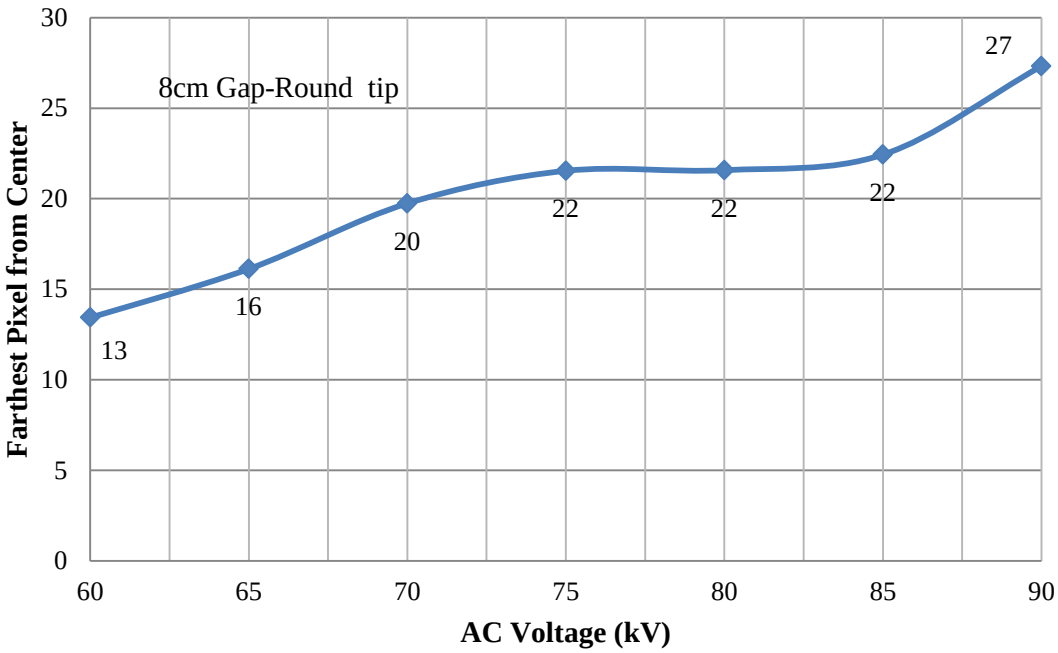

Figure 5.9. Trend of discharge propagation with respect to applied voltage for 8 cm electrode gap of round-tip electrode

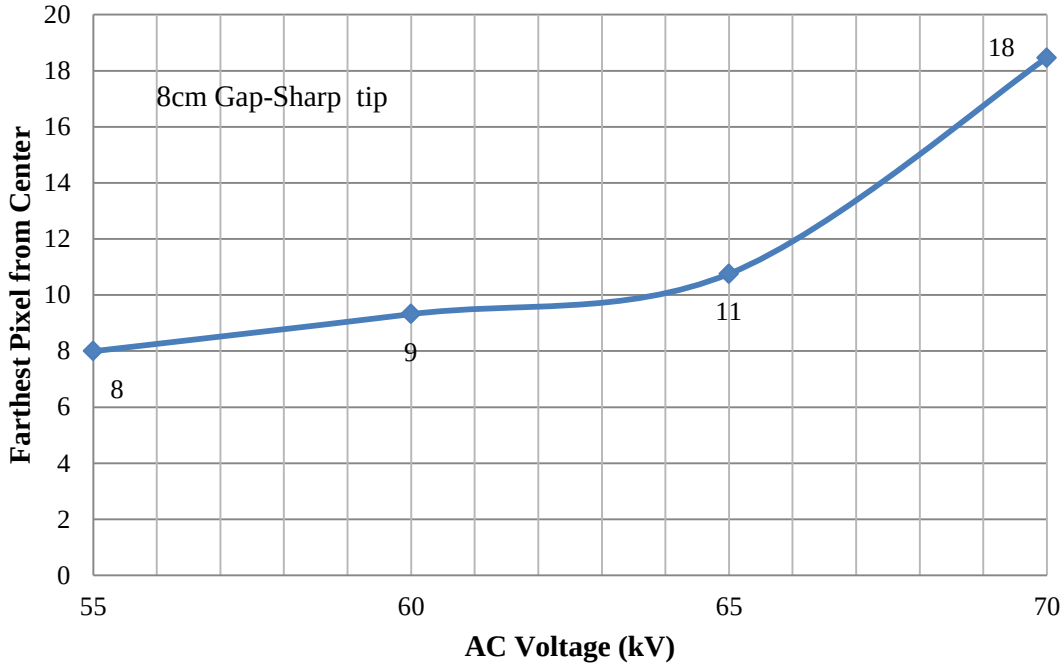

Figure 5.10. Trend of discharge propagation with respect to applied voltage for 8 cm electrode gap of sharp-tip electrode

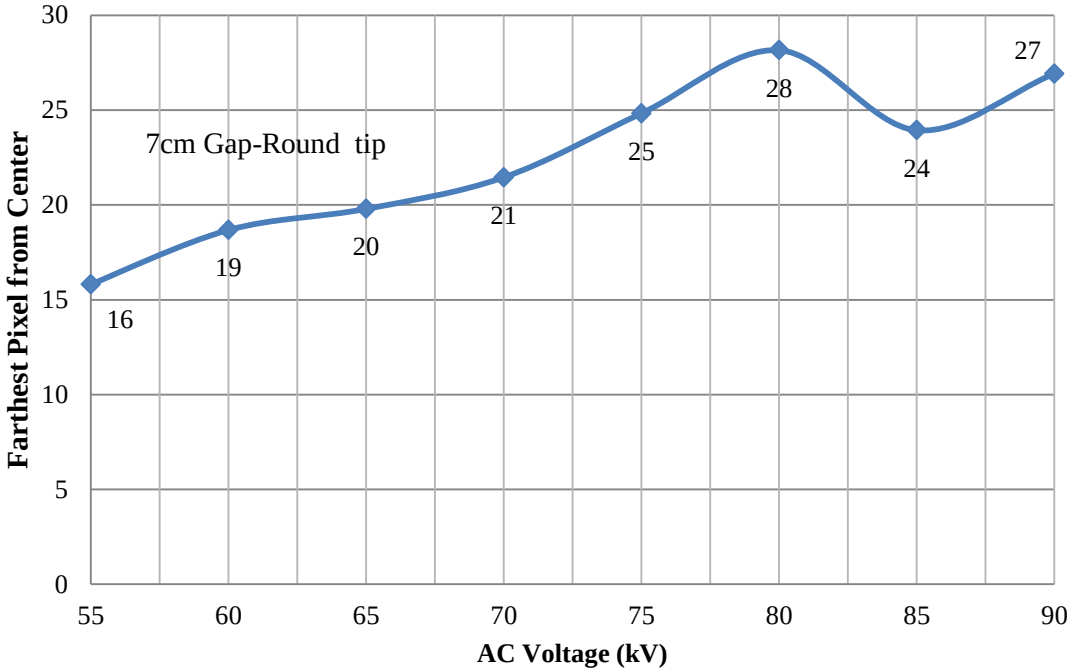

Figure 5.11. Trend of discharge propagation with respect to applied voltage for 7 cm electrode gap of round-tip electrode

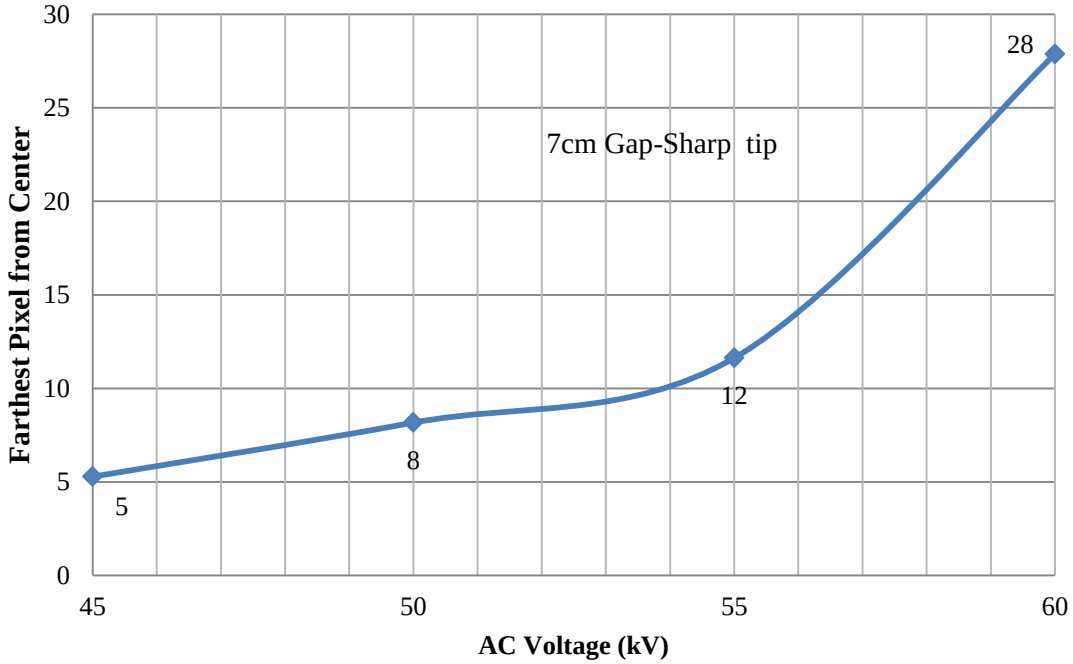

Figure 5.12. Trend of discharge propagation with respect to applied voltage for 7 cm electrode gap of sharp-tip electrode

5.2.3 Intensity

Intensity for sharp tip electrode is shown in the Table 5.5. This table shows that the discharge initiates sooner for smaller electrode gap. In smaller electrode gaps, it is not possible to initiate partial discharges. The value of luminance belongs to visible discharge area is calculated as the maximum value of each frame then the average values of all frames are taken into account.

Table 5.5. Intensity of discharge light with respect to applied voltage for different electrode gaps of sharp-tip electrode

	Applied voltage [kV]						
Electrode Gap [cm]	**40**	**45**	**50**	**55**	**60**	**65**	**70**
5	41	83	BD	BD	BD	BD	BD
6	-	55	71	75	BD	BD	BD
7	-	45	58	72	132	BD	BD
8	-	-	-	53	60	71	86

Since the electric field intensity is stronger where the curvature radius is small, it was expected to have stronger electric field for sharp-tip rod electrode compared to round one. This fact can be observed in light intensity Table 5.5 and 5.6.

Table 5.6. Intensity of discharge light with respect to applied voltage for different electrode gaps of round-tip electrode

	Applied voltage [kV]									
Electrode Gap [cm]	**45**	**50**	**55**	**60**	**65**	**70**	**75**	**80**	**85**	**90**
5	37	42	53	59	BD	BD	BD	BD	BD	BD
6	-	-	31	37	41	BD	BD	BD	BD	BD
7	-	48	54	59	63	71	78	76	89	99
8	-	-	-	40	48	61	68	79	82	67

The intensity of light belongs to discharge zone for both round-tip and sharp-tip electrodes for different electrode gaps from 8 cm and 7 cm are shown in Figs 5.13-16. The number of corona observations is decreased for smaller electrode gaps. It is obvious that, intensity of light is getting higher when the voltage level is increased. Moreover, the value of light intensity is always bigger for sharp tip electrode under same voltage. This trend is compatible with theory of electrical field intensity that electrical field is stronger where curvature radius is smaller i.e. electrode is sharper. Numerical solution which are explained in the Chapter 3 also support those results.

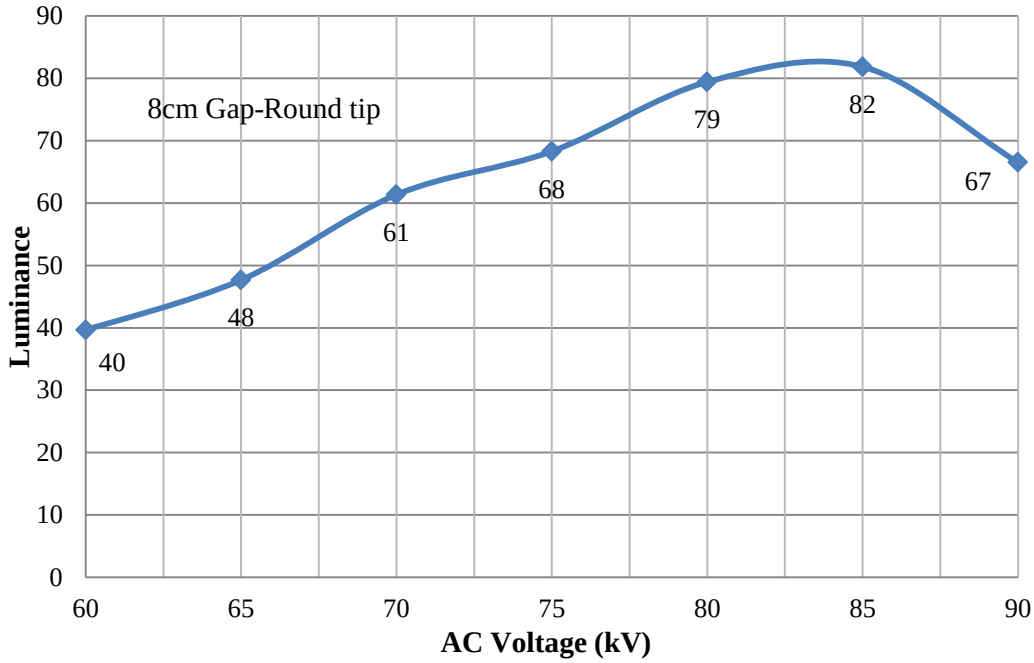

Figure 5.13. Trend of light intensity with respect to applied voltage for 8 cm electrode gap of round-tip electrode

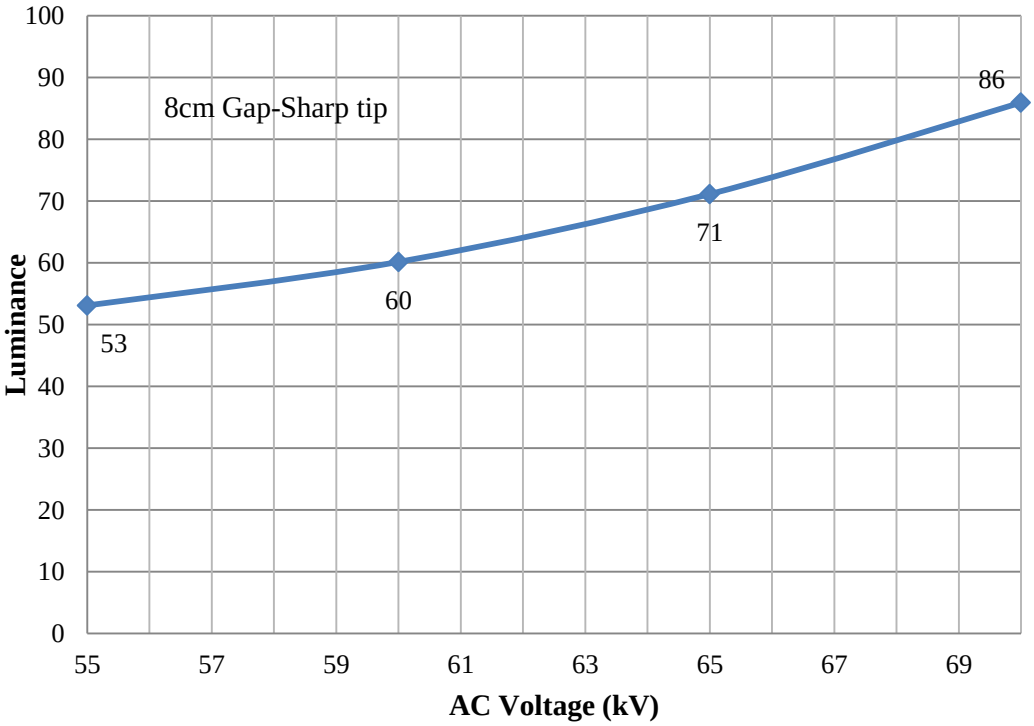

Figure 5.14. Trend of light intensity with respect to applied voltage for 8 cm electrode gap of sharp-tip electrode

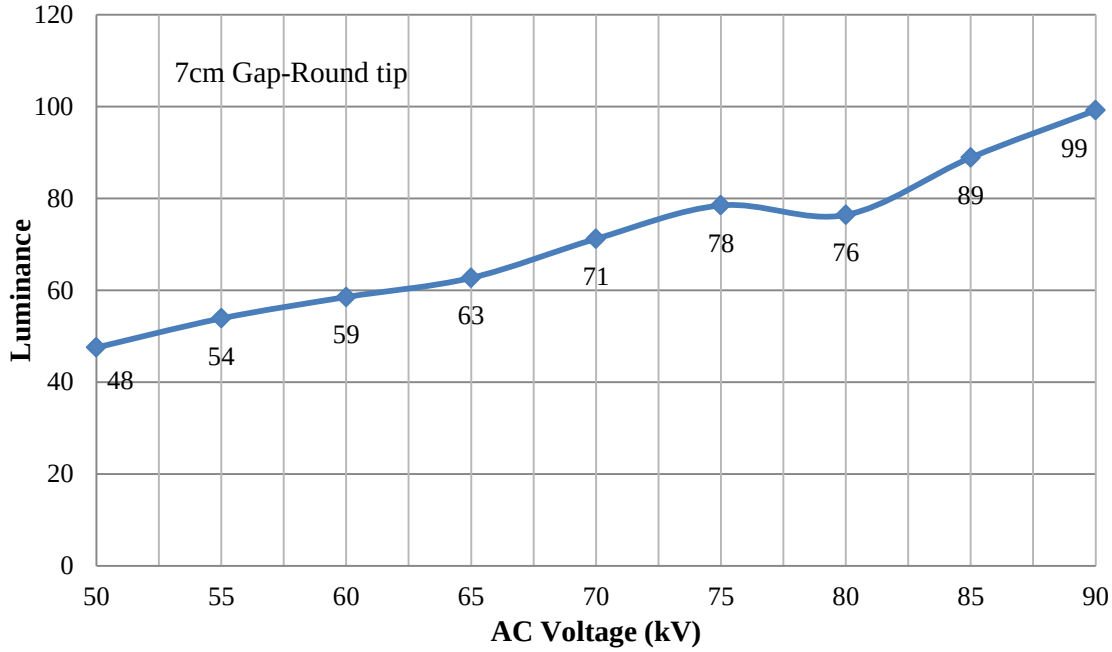

Figure 5.15. Trend of light intensity with respect to applied voltage for 7 cm electrode gap of round-tip electrode

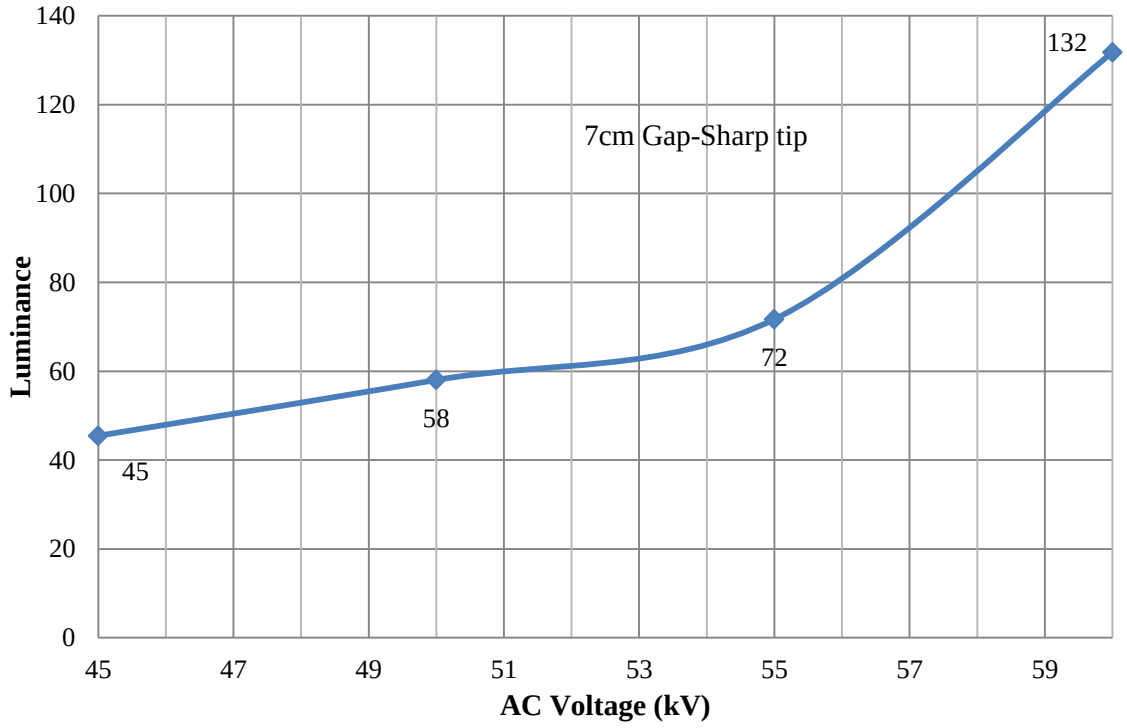

Figure 5.16. Trend of light intensity with respect to applied voltage for 7cm electrode gap of sharp-tip electrode

5.3 Discussion

The experimental study shows that, all the measurements are compatible with theoretical background except minor irregularities. According to Gauss' law (Eqs.3.4-9) electric field is stronger where the charge density is bigger. That means, under same level of voltage for the same electrode gap, source charges are closer to each other at sharp points with smaller curvature radius. Therefore, electric field is stronger for sharp-tip electrode compared to the round-tip electrode. The light intensity increases with electric field which means when the electrical field is stronger the light is brighter. Experiments reveal that, light is brighter, light intensity is higher for the sharp-tip electrode which has higher electric field intensity. The result of numerical solution also supports the experimental study. The numerical solution shows that, the electric energy density (J/m^3) for sharp-tip electrode is higher compared to the round-tip electrode under same voltage (Tables 3.1 and 3.2). Calculated energy density is compatible with the energy characteristic of light. The area growth of discharge is smaller for sharp-tip because electric field lines are closer in this profile. Similarly, light propagation is smaller for sharp-tip electrode. Obviously, the distance between furthest pixel of light to center increases when the area growth gets bigger. Also according to Eq. 3.22 electric field has inverse relation with electrode separation that electric field is stronger for smaller gap under same level of voltage.

It should be noted again that experimental results is supported by the numerical solution. Electric field increases when the applied voltage is increased as expected. But in experiments, results show some irregularities due to unpredictable flashovers.

Chapter 6

CONCLUSION AND FUTURE STUDY

6.1 Conclusion

In this study, a visual recognition of corona discharge by video processing has been carried out. Two rod-type electrodes with different profiles are designed. For the rod electrodes, different curvature radius at the tip is used. Using those profiles, rod-plane electrode arrangement is installed to be tested. Experiments are conducted at approximately standard ambient conditions . The images of visible discharge light on the rod electrodes are recorded and by video processing they are translated into three quantifiable parameters: area growth, propagation and light intensity of discharge zone. Strong relationship between those parameters and applied voltage level has been observed. All of the measurements and calculations are compatible with theoretical background.

This study shows that, with the recent developments in signal processing techniques, it is possible to analyze discharges by their light. It should be noted that light characteristics of corona; area growth, light propagation and light intensity are quite distinctive which makes a visual recognition accurate.

This study covers visual recognition only for corona discharge. By using different electrode configurations, dataset can be expanded to generate different discharge

types such as flashover, breakdown, etc. In this way, it is possible to classify different discharges using their visible light characteristics.

Predicting the voltage level, electric field intensity around a conductor by light parameters of a discharge is also possible. Analysis and predictions in a power system with non-electrical measurements will be very helpful in the future by using new techniques of image processing. Because in this way, necessary economic or technical measures can be taken without interrupting the entire system.

This study is a minor step for on-site fault detection by corona light and planned to be improved.

6.2 Future Studies

For the next step, effect of ambient conditions will be investigated in a controlled environment. Moreover, other types of camera such as UV camera and infrared camera will be tested to have more accurate data because of their sensitivity. Online identification of discharge is also possible by video processing method, which is very helpful to monitor discharge activity in an operating power system.

This study shows that, image processing and video processing applications can be good tools for PD analysis studies. Detection, classification, localization of PD, monitoring a power system and remote sensing are possible by this method.

REFERENCES

[1] Tanaka, T. (1986). Internal partial discharge and material degradation," *IEEE Transactions on Electrical Insulation*, vol. EI-21, no. 6, pp. 899-905

[2] Seanor, D. A. (1982). Electrical Properties of Polymers. *Academic Press*, Inc., ch. Chapter 1, pp. 1-10

[3] Kuffel, E., Zaengl, W. S., & Kuffel, J. (2005) *High voltage engineering: fundamentals, Published by Elesvier*, ISBN 0-7506-3634-3, second edition

[4] Boggs, S. A. (1990). Partial discharge. iii. cavity-induced PD in solid dielectrics, *IEEE Electrical Insulation Magazine*, vol. 6, no. 6, pp. 11-16, 19-20

[5] Okamoto, T., Kato, T., Yokomizu, Y., Suzuoki, Y. & Tanaka, T. (2001). PD characteristics as a stochastic process and its integral equation under sinusoidal voltage, *IEEE Transactions on Dielectrics and Electrical Insulation*, vol. 8, no. 1, pp. 82-90

[6] Hozumi, N., Nagae, H., Muramoto, Y., Nagao, M. & HengKyun, X. (2001) Time-lag measurement of void discharges and numerical simulation for clari_cation of the factor for partial discharge pattern, *Proceedings of International Symposium on Electrical Insulating Materials*, pp. 29-32

[7] Hikita, M., Yamada, K., Nakamura, A., Mizutani, T., Oohasi, A. & Ieda, M.

(1990). Measurements of partial discharges by computer and analysis of partial discharge distribution by the monte carlo method, *IEEE Transactions on Electrical Insulation*,vol. 25, no. 3, pp. 453-468

[8] Suzuki, H., Aihara, K. & Okamoto, T. (2004). Complex behavior of a simple partial discharge model, *EPL (Europhysics Letters)*, vol. 66, no. 1, p. 28

[9] Dodd, S. J., Champion, J. V., Vaughan, A. S., Sutton, S. J. & Swingler, S. G. (2003). The influence of morphology on electrical treeing in polyethylene blends, *IEEE Proceedings of Science Measurement and Technology*, vol. 150, no. 2, pp. 58-64

[10] Morshuis, P. H. F. (2005). Degradation of solid dielectrics due to internal partial discharge: some thoughts on progress made and where to go now, *IEEE Transactions on Dielectrics and Electrical Insulation*, vol. 12, no. 5, pp. 905-913

[11] Van Brunt, R.J. (1994). Physics and chemistry of partial discharge and corona, *IEEE Transactions on Dielectric and Electrical Insulation*, vol. 1, no.5, pp. 761–784

[12] Van Brunt, R.J. (1991). Stochastic properties of partial discharge phenomena, *IEEE Transactions on Dielectric and Electrical Insulation*, vol. 26, no.5, pp. 902–948

[13] Erning, L. (1998). The study of the characteristics of corona discharge, *High Voltage Apparatus*, vol. 6, pp. 16–21

[14] Phillips, A. J., Childs, D. J. & Schneider, H. M. (1999). Aging of Non-ceramic Insulators Due to Corona from Water Drops, *IEEE Transaction on Power Delivery*, vol. 14, no.3, pp. 1081–1089

[15] Edin, H. (2001). Partial discharges studied with variable frequency of the applied voltage, PhD Thesis, Royal Institute of Technology (KTH), Stockholm, Sweden

[16] SABAT, A. (2011). Simulation of partial discharge in high voltage power equipment, *Master Thesis, National Institute of Technology*, Rourkela, Rourkela-769008, India

[17] Boggs, S. A. (1990). Partial Discharge: Overview and Signal Generation, in *IEEE Electrical Insulation Magazine*, vol. 6, pp. 33-39.

[18] Stone, G.C. (2005). Partial Discharge Diagnostics and Electrical Equipment Insulation Condition Assessment, dielectrics and Electrical Insulation, *IEEE Transactions on Volume*: 12, Issue: 5. Page(s): 891 – 904

[19] Kemp, I. J. (1995). Partial discharge plant-monitoring technology: Present and future developments, *IEE Proc.-Sci. Meas*. Technology, vol. 142, pp. 4-10

[20] Duval, M. (1989). Dissolved Gas Analysis: It Can Save Your Transformer, *in IEEE Electrical Insulation Magazine*, vol. 5pp. 22-27.

[21] Bartnikas, R. (2002). Partial Discharge their mechanism, Detection and Measurement, *IEEE Transactions. Electrical Insulation*., Vol. 9, pp. 763-808

[22] Imad U.K., Wang, Z., Cotton, I. & Northcote, S. (2007). Dissolved gas analysis of alternative fluids for power transformers, *Electrical Insulation Magazine, IEEE* Volume: 23, Issue: 5, 5 – 14

[23] Karmakar, S., Roy, N. K. & Kumbhakar, P. (2009). Partial Discharge Measurement of Transformer with ICT Facilities, *Third International Conference on Power Systems*, Kharagpur, India

[24] Lazarevich, A. (2003). Partial Discharge Detection and Localization in High Voltage Transformers Using an Optical Acoustic Sensor Master thesis, *Virginia Polytechnic Institute and State University*

[25] Wenjun, Z., Jianbin, W., Minghua, M., Bin, M. & Xiao, Y. (2009). Research on quantification of AC corona discharge intensity of rod-plane gap based on UV digital Image Processing, *IEEE conference, Power and Energy Engineering Conference,* Asia-Pacific.

[26] Pinnangudi, B., Gorur, R. S. & Kroese, A. J. (2005). Quantification of corona discharges on nonceramic insulators, *IEEE Transactions on Dielectric and*

Electrical Insulation, vol. 12, no.3, pp. 513–523

[27] Cheng, D. (1983). Field and wave electromagnetics, ch3, pp.65-90

[28] www.physicclassroom.com/class/estatics/lesson-4

[29] Malik, N. H., Al-Arainy, A. A. & Qureshi, M. I. (1998). Electrical insulation in power systems, ch2, pp.36-45

[30] Kolenderli, O., Onal, E. & Altay, O. (2001). Computing the corona onset and the utilization factor of rod-plane electrode by using charge simulation method, *IEEE conference, Electrical insulation conference*, Cincinnati, USA

[31] Reddy, J.N. (2005). An introduction to the finite element method, third edition.

[32] Gonzalez, R.C., Woods, R. E. & Eddins, S. L. (2009). Digital Image Processing Using MATLAB, second edition.